PON Ricerca e Innovazione 2014- 2020

Unione Europea

Ministero dell'Istruzione, dell'Università e della Ricerca

UNIVERSITÀ DEGLI STUDI DI NAPOLI FEDERICO II

PhD thesis in Industrial Products and Process Engineering

(XXX Cycle)

"*Fabrication of in vitro epithelial tissues as a testing platform for drug delivery systems*"

PhD Student

Dr.ssa Angela Langella

Coordinator

Prof. Giuseppe Mensitieri

Supervisor

Prof. Paolo A. Netti

Advisors

Giorgia Imparato, PhD

Raffaele Vecchione, PhD

Vincenza De Gregorio, PhD

2014/2017

I do not know how the world can judge me, but it seems to me only to be a child playing on the beach, and to have enjoyed having to find occasionally a rock or shell more beautiful than usual, while the ocean of truth lay uncharted before me.

(Sir Isaac Newton)

To My Mother,

The one who has shown me

To never give up

To believe in my dreams

and

to make they come true.

To Simone,

My Promised Husband

The one who has always believed in me,

The one who has always supported me in all my choices.

My Half,

My only Love,

My Forever.

Table of Contents

List of abbreviations and symbols

ALI	Air Liquid Interface
ATCC	American Type Cell Culture
CaCo-2	Colorectal Adenocarcinoma Cells
CT	Chitosam
CTRL	Control
CUR	Curcumin
CRCs	Colorectal Cancer
CLN	Curcumin Loaded Nanocapsules
DMEM	Dulbecco's Modified medium
DPBS	Dulbecco's Phosphate buffered saline
ECM	Extracellular Matrix
FBS	Fetal Bovine Serum
GC	Glycol Chitosan
GI	Gastrointestinal
GCNAC	Glycol thiolated chitosan
HBSS	Hank's balanced solution
HDFs	Human dermal fibroblasts
LBL	Layer by Layer
LPS	Lipopolysaccharide
MEM	Minimum Essential Medium
NAC	N-Acetyl-L-Cystein
NEEA	Nonessential amino-acids
NMR	Nuclear Magnetic Resonance
NPs	Nanoparticles
O/W	Oil in water
PC	Policarbonate
PDMS	Poly-dimethyl-siloxane
PET	Polystyrene
PLGA	Polylactic-co-glycolacid
PXL	Paclitaxel
RT-PCR	Real Time Polymerase Chain Reaction
RBITC	Rhodamine B isothiocyanate
TE	Tissue engineering
TEER	Trans-epithelial-electric-resistance
TJs	Tight junctions
µTP	Micrometric tissue precursor
2D	Bidimensional
3D	Threedimensional

General Abstract

In the last years, tissue engineering (TE) has advanced offering the potential for regenerating almost every tissue and organ of the human body. Three dimensional (3D) human tissue models can provide a good platform for pharmacological screening and drug delivery rather than traditional bidimensional (2D) cell culture or animal models. In native tissues the extracellular matrix (ECM) promotes the crosstalk between cells, and is responsible of several fundamental pato-physiological processes. For this reason, tissue engineering is moving forward the development of *in vitro* models in which endogenous ECM is present. In the perspective of using *in vitro* tissues as testing platform. Nowadays there is an overlapping between tissue engineering and nanomedicine since they share the common application to improve the new molecules screening *in vitro* and the pre-clinical testing. Nanomedicine and nanofabrication allow to create miniaturized release-based systems such as nano-bio-capsulates while novel tissue engineering processess allow to building up *in vitro* tissues and organ mimicking their *in vivo* counterpart. Nanomedicine relies on the fundamental principles of tissue engineering as well as the tissue engineering field favors from continuous progress in nanomedicine. Indeed, due to the complexity of these tissues, studying and analyzing possible strategies to implement specific nanocarriers is becoming more and more challenging. The big challenge is engenneering capsules able to specifically target a certain organ of interest and, then, ensure an effective *in situ* controlled release.

The aim of my PhD work is to effectively bridge nanomedicine and tissue engineering. Particularly, on the one hand-side, this work focused on the realization of functionalized nanoparticles that are able to transport lipophilic drug preventing their early degradation. On the other side, a 3D intestinal diseased model as a platform for drug screening was realized.

We created nanocapsules starting from an oil-in-water (O/W) nanoemulsion coated with a polysaccharide layer film, *i.e.* a glycol-modified chitosan, and subsequently curcumin and paclitaxel were loaded. These compounds are usually unlikely water-soluble. In particular, curcumin can be involved as a factor for preventive therapy while Paclitaxel is included in farmaceuticals for treatment of colorectal carcinoma. The final nano-carriers are completely biocompatible and biostable.

In the first part, I investigated the enhancement of the effect of curcumin loaded in our system across monolayers of intestinal epithelial cells (CaCo-2) in transwell culture. Such *in vitro* platform is suitable for evaluating the functionality of the nano-carrier and its specificity towards the mucosal epithelial layer. As an applicative example, the investigation of the anti-inflammatory effects exerted by the encapsulation of curcumin was carried out.

In the second part, I developed a more complex *in vitro* cellular model. This is relevant for creating a unique 3D tumoral intestinal model capable of mimic physiological i*n vivo* diseased architecture. Under these conditions, it was possible to precisely evaluate the anti-tumoral effets of paclitaxel in nanocapsules.

In conclusion, I started from a 2D system to test the internalization capability and the efficacy of nanocapsules and then I moved towards

the development of a pathological 3D system and implemented the aforementioned internalization of nanocapsules loaded with potential chemioterapeutics (paclitaxel).

Effectively, this work contributes to develop a future high throughput platform for drug screening of a variety of nano-carriers against tumoral-like cellular components.

Chapter 1: State of art

Tissue engineering meets nanomedicine

Introduction

The main function of the small intestine is the absorption of essential nutrients, water and vitamins. Moreover, it constitutes a barrier protecting us from toxic xenobiotics, pathogens and drugs. For a better understanding of these processes, the development of a valid intestinal *in vitro* model as a platform for drug delivery is necessary for more accurate pharmacological and pathological investigation such as transport mechanisms and barrier function.

1.1 Intestinal epithelium: structure and function

Human small intestine, which includes the duodenum, jejunum and ileum, is a convoluted tube that is, on average, 2.5 cm in diameter and 3 m long [1] The human small intestine possesses highly complex 3D microenvironments that achieve the maximum efficiency of absorption thanks to the presence of circular folds and villi (Figure 1.1a). The small intestine submucosa and mucosa form valvulae conniventes or Kerckring's folds that protrude into the lumen transversely and increase the retention time of chyme. These permanent ridges, begin to appear near the proximal portion of the duodenum and disappear nearly completely in the distal ileum. [2] On the surface of these structures there are some protrusions known as intestinal villi. Each villus is about 0.5 mm high and there are 30 villi per mm^2 (Figure 1.1b). [1-3] Between each villus there are the invaginations named crypts. Intestine stem cells can differentiate into four different intestinal epithelial type of cells, which are the enterocyte or absorptive cells, goblet, enteroendocrine and Paneth

cells. Although Paneth cells reside within the stem cell niche at the bottom of the crypt, the other three types of intestinal epithelial cells migrate toward the tip of the villus, forming a columnar epithelial monolayer that covers the intestinal mucosa. The crypt and villus structures generate chemical gradients that affect the epithelial cell physiology. On the basolateral surface there is the blood flow. In the lumen there are also many commensal bacteria with a density increasing from 10^3 organisms per ml of luminal contents in duodenum to 10^9 per ml of luminal contents in the distal ileum. [4] Within this dynamic and complex environment, the small intestine epithelium has the most vigorous renewal process in adult epithelial tissues, with the epithelial monolayer regenerating every 5 days.

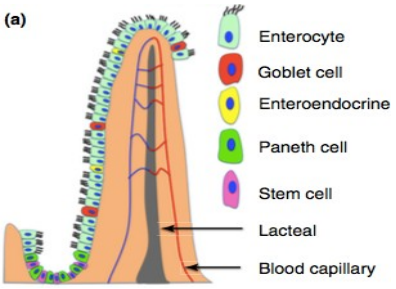

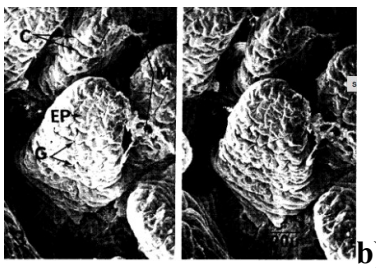

b)

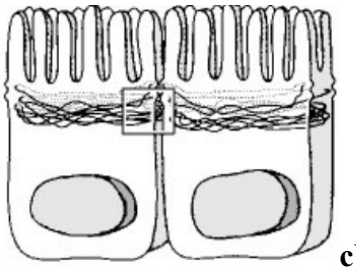

c)

Figure 1.1:a) Illustration of human small intestine epithelium on crypt–villus axis. Adapted from [1] **b)** SEM of human small intestine villi. Stereo pair scanning micrographs showing a group of villi. The great depth of focus of the sem is clearly demonstrated. Epithelial cells (EP), globet cell orifices (G), corrugations (C), crypt mouths (CM) and mucus (M) COPYRIGHT ref [3]. **c)** Continuous cell-cell contact is made at the apical end of the lateral interspace where a ring of bidirectional actin filaments is concentrated Adapted from [5]

The fundamental function of the intestinal epithelium is to act as a barrier that limits interactions between luminal contents such as the intestinal microbiota, the underlying immune system and the remainder of the body, while supporting vectorial transport of nutrients, water and waste products. [5] Epithelial barrier function requires a contiguous layer of cells as well as the junctions that seal the paracellular space between epithelial cells. Epithelial cell layers are interconnected by tight junctions (TJs), which are localized within apico-lateral membranes. The proteins that form TJs are regarded to provide a static barrier, determining epithelial properties. Compromised intestinal barrier function has been associated with a number of disease states, both intestinal and systemic. [6] The intestinal epithelium forms an important physiological barrier in the gastrointestinal (GI) tract but this barrier can be compromised by a wide range of substances including drugs, microbes, and dietary disorders including inflammatory bowel disease and in the other cases colon rectal cancer. For this purpose, a lot of *in vitro* models have been developed in order to understand the drug absorption and trasport. [7]

1.2 Realization of the intestinal epithelium equivalent in transwell as a platform for drug delivery test: from 2D to 3D models

The first *in vitro* intestinal epithelium that marked a promising passage from 2D model to 3D model, was realized for detailed studies of drug transport by using cultured monolayers of epithelial cell lines grown on semipermeable membranes called *Transwell.*(Figure 1.2) [8-9]

These cells, known as CaCo-2, a human colon carcinoma cell line, which exhibits features similar to human intestinal epithelium, are able to form a confluent enterocytes-like cells [10] and for this purpose are used for *in vitro* studies. CaCo-2 model has been developed as a powerful *in vitro* tool in the early assessment of human drug permeability and is even approved by regulatory agencies for biowaver applications (*i.e. in vitro* tests in lieu of *in vivo* animal experiments). CaCo-2 cells represent a more formidable barrier to drug absorption than the upper regions of the intestine, which is where the majority of oral drugs permeate into the body. The first study attempting to correlate passive drug permeability in CaCo-2 monolayers with drug absorption in humans after oral administration suggested that the cell monolayers might be used to identify drugs with potential absorption problems. [11] Many researchers have sought to improve upon the existing unicellular model. It is hoped that this will result in a more relevant and predictive model for researchers to test new drugs but also to dissect cellular cross talk and to probe cell-matrix interactions.

Transwell systems are based on a porous polystyrene (PET) or polycarbonate (PC) membrane to study of transport mechanisms across the intestinal epithelial barrier as well as the investigation of the influence of target substances on barrier integrity. However, this artificial setup reflects only limited aspects of the physiology of the native small intestine and can pose an additional physical barrier. The 2D *in vitro* small intestine model has been widely recognized as a very useful screening tool that has not only greatly reduced animal use but also facilitated the drug discovery and preclinical development processes.

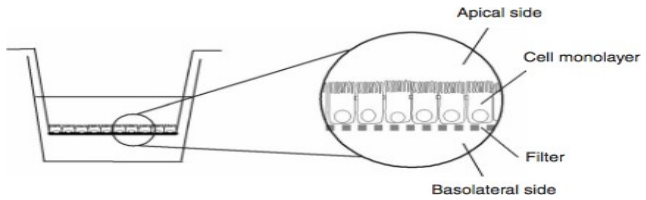

Figure 1.2: Transwell permeable support: Caco-2 monolayer grown on a permeable filter support.

The succesful promotion of a commercial drug requires significant speculation of time and financial resources wherein latestage failures become a reason for catastrophic failures in drug discovery.

The innovation in technologies, need to give reliable prediction of efficacy, and more importantly, toxicology of the compound early in the drug discovery process before clinical trials.

In vitro studies still require an improvement of *in vitro-in vivo* correletions and for this purpose, due to their ability to mimic spatial and chemical attributes of native tissue, (3D) tissue models have

demonstrated to provide better results for drug screening. However, *in vivo* cells reside in a 3D environment surrounded by other cells and the ECM that play an important role in a living tissue. Recent studies indicated that cell-cell interaction and cell-extracellular matrix communications are key factors between 2D and 3D system as well as between different 3D systems. [12]. The majority of existing cell-based drug assays utilizes the 2D monolayer culture method in which cells are attached on flat or rigid substrate comprised of glass or polystyrene. In this condition, cells proliferate at a rapid rate to a sheet-like confluency but cannot replicate the microvillus polarization. The absorptive surface in terms of area is not enough for a valid predictive studies. However, owing to their inability to achieve the complexity of *in vivo* cell and tissue organization, they do not adequately recapitulate healthy phenotype.

Animal models also fail to recapitulate much of human physiology and disease. [13] Because of the importance of the gastrointestinal (GI) tract to health and disease, many *in vitro* and *in vivo* animal models and human tissue models of the GI tract have been developed. [14-16]

1.3 Tissue engineering (TE) for drug delivery

Over the last years, Tissue Engineering (TE) has established in the biomedical and scientific scenario as a new emerging field consisting of several interdisciplinary applications that combine the principles and methods of life science with those of engineering, aiming at repairing or regenerating portions or of whole biological tissue and organs (bone, cartilage, bladder, skin, cornea, blood cells, muscle, liver, pancreas, intestine, etc.). [17-20] The purpose of TE research is very clear: establishing a new clinical technology that makes possible medical applications for diseases that have been too difficult to be cured by existing methods. Initially, it was thought that the principles of TE could be applied only virtually, but today it is known that many applications are widely used not only in tissue regeneration but also in the industrial field. [21-22] The biological environment is made up of cells, cellular signaling and ECM. The cells are the core of the tissue for istance, to explicate their funtions they require an adequate system of signal transduction. The ECM is composed also of collagen and elastin fiber network synthetized by the cells themselves and secreted in the extracellular space. Single cells, without a three-dimensional guide, are indeed not able to organize themselves in a 3D tissue with its complex architecture, since the only cell proliferation is not sufficient. Single cells need a 3D support, defined as “scaffold”, whose main function is to support and control cellular processes, as well as proliferation, differentiation and synthesis of organic molecules and mediators, known as growth factors, which act in an autocrine and paracrine pathways on cellular processes. [23] As shown in literature, the first 3D tissue models

reproduced *in vitro* were those which are frequently injured [24] as skin, cartilage or bone. In contrast there are other tissues (e.g gut, liver, cervix) which are enginereed for the investigation of organ targeting, drug delivery and drug screening.

1.3.1 *In vitro* 3D intestinal models: from decellularized animal scaffold models to artificial topography models

There are a lot of intestinal epithelial in *vitro* platforms used for drug delivery systems that replaced the conventional 2D *in vitro* models like transwell model. One of these is the reproduction of a 3D small intestine created *in vitro* by utilizing decellularized small animal intestine segments. [26] For example, CaCo-2 cells and human microvascular endothelial cells were cultured on the apical and basolateral sides of a decellularized porcine jejunal scaffold. [27] Biological scaffolds from decellularized tissues currently offer the highest comparability to tissues *in vivo*. Among these scaffolds, the BioVaSc-TERM®, a decellularized porcine gut segment, demonstrated to be applicable as a platform for the generation of various tissues equivalents. [28] Hence, the scaffold can be used to generate vascularized tissue equivalents by reseeding the vessels with human endothelial cells and the subsequent perfusion using bioreactor systems. [29] The BioVaSc-TERM® has already been tested as a vascularized implant in preclinical studies and employed as an autologous airway patch. [30] However, since the scaffold is complex and not all features are needed in mid- or high-throughput testing strategies, the BioVaSc-TERM® need to be adapted to the

requirements of *in vitro* drug testing. [31] Walles *et al*. also developed an alternative primary human small intestinal tissue model. This novel approach combines previously established gut organoid technology with a natural (ECM) based on porcine small intestinal scaffold (SIS). Intestinal crypts from healthy human small intestine were expanded as gut organoids and seeded as single cells on SIS in a standardized transwell-like setting. [32] Additionally, a decellularized rat intestinal scaffold with villus–crypt structures and vasculature has been obtained by using detergent–enzymatic treatment, and its potential for recreating functional intestine tissue was demonstrated. [33] In particular, reducing animal testing in drug development, is one of the first aim for the scientists. Furthermore, the requirement of using animal tissue makes these methods less practical for preclinical drug studies than other *in vitro* models. Animal models also fail to recapitulate much of human physiology and diseases. In the last two decades with the development of microfabrication and other biomaterials, fabrication techniques, biomimetic topography has been integrated into *in vitro* intestinal models to represent human small intestine 3D features. The artificial topography for reproducing 3D small intestine models has been largely developed. Indeed, through the use of photolithography, human small intesine crypte were ribuild. [34-35] Wang *et al.,* suggesting that the influence of micron-scale (100mm) crypt-like micro-well topography on intestinal cell behavior it is important to determine whether the unique topography of intestinal crypt-villus unit plays an important role in regulating intestinal cells. [36] CaCo-2 cells were cultured on poly-dimethylsiloxane (PDMS) substrates with biomimetic topography (micro-well arrays). It was found that

intestinal crypt-like topography affects CaCo-2 spreading, migration, metabolic activity, as well as cell differentiation. This study outcomes the influence of topography substrates on cells. Elements for biomimetic scaffolds can be ultimately designed for intestinal tissue engineering. Compared with 2D flat substrates (Figure 1.3), CaCo-2 cultured on PDMS substrates with crypt-like topography exhibited higher mitochondrial activity and lower alkaline phosphatase activity like *in vivo*. [37] Wang *et al.* published another study where a biomimetic intestinal cell culture system composed of type I collagen based permeable cell culture membranes incorporating both micron-scale intestinal crypt-like topography and nanometer scale topography was fabricated. In this case, transepithelial electrical resistance (TEER) values were found to be slightly lower for CaCo-2 monolayers cultured on topographically modified collagen membranes relative to flat collagen controls, suggesting that crypt-like topography might affect tight junctions of the CaCo-2 monolayer. [38]

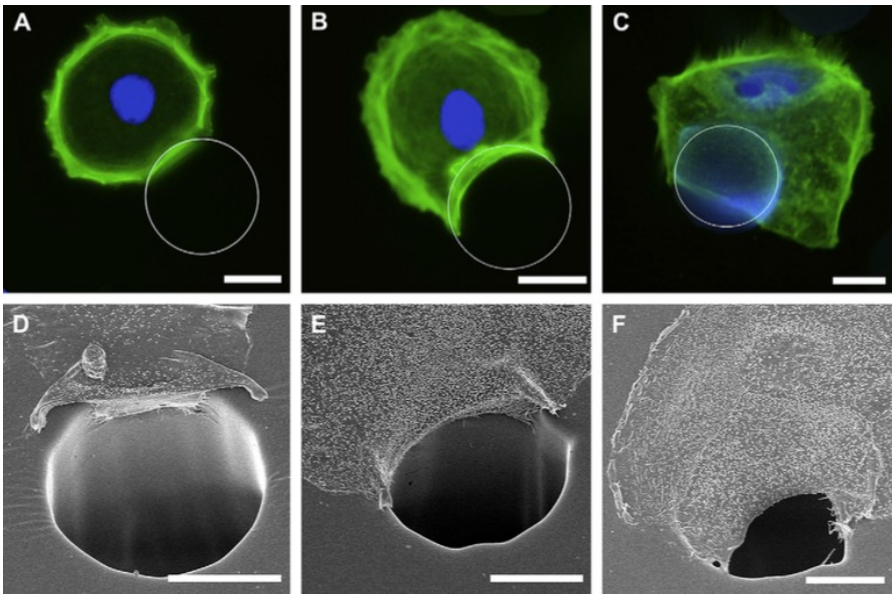

Figure 1.3. CaCo-2 cultured on PDMS substrates with crypt-like topography: F-actin staining **(A,B,C)** and SEM **(D,E,F)** of Caco-2 cells interacting with 50 mm well structures as they spread across the wells, 24 h after initial seeding. The scale bar corresponds to 25 mm. [Adapted from Wang *et al.,* 2009]

Wang *et al.* (Figure 1.3) utilized to build up villus scaffolds is poly(lactic-co-glycolic acid) PLGA, but porous PLGA villous structures had considerably larger basal areas than human small intestine vill, however owing to the resolution limitation of this technique, could not represent dimensions and density of villi relevantly. [39] Sung *et al* showed that, by combining laser ablation and sacrificial molding techniques, a collagen villous scaffold was fabricated with 0.5 mm villous height and 25 villi per mm^2 density, with striking similarity to the human jejunal villi. [40] They proposed a hydrogel scaffold mimicking the microscale 3-D geometries of biological tissues. This method offers several advantages over currently existing methods for microfabrication of hydrogels. Using

alginate as a sacrificial layer is particularly advantageous since the alginate dissolving process is physiologically mild, and therefore compatible with applications involving cell (Figure 1.4). Although the collagen scaffold did not exhibit variable transport characteristics for different small molecule drugs, the scaffold itself became a significant transport barrier for the rapidly absorbed drug antipyrine, which is absorbed through a transcellular pathway. Hence, this 3D model not be used to test a wide range of drugs with broad permeability coefficients. Ingeber *et al.* demonstrated that the engineered villi exhibit specialized cell and tissue functions, including elevated mucus production and enhanced CYP3A4 drug metabolizing activity (Figure 1.5).

Another type of 3D model consists of multiple layers of relevant cell types, including a flat monolayer of Caco-2 on a gel containing dendritic cells or macrophages. [41] Generally, to form these models, a thicker layer of collagen protein matrix than used on conventional 2D models was coated on a cell culture insert. Although the flat collagen matrix does not capture structural features of the small intestine 3D microenvironment, the integration of immune components in the collagen matrix makes this model a useful *in vitro* tool for studying inflammatory bowel diseases.

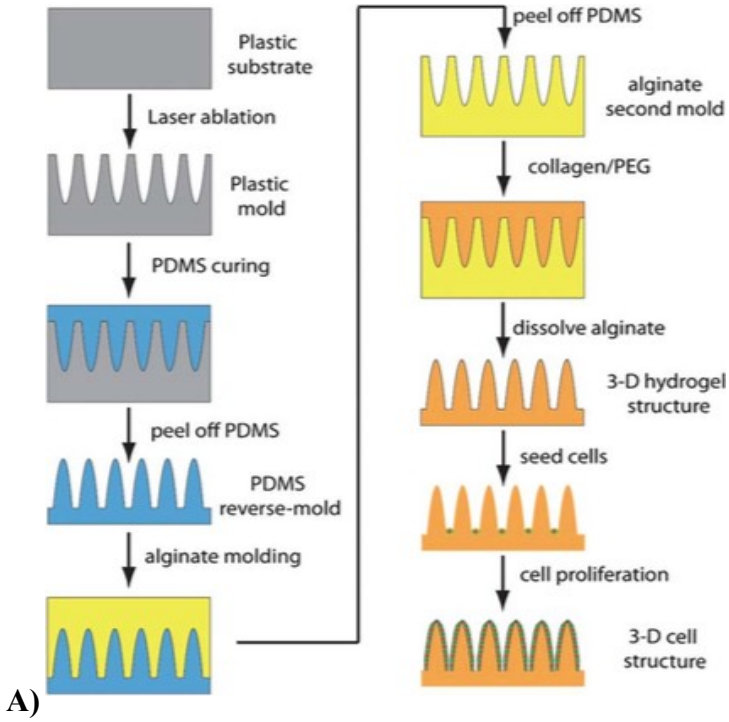

Figure 1.4 Hydrogel scaffold mimicking the microscale 3-D geometries of biological tissues: A) Overall fabrication process. The first plastic mold is created by laser ablation, from which the PDMS reverse-mold is created. The alginate second mold is made from the PDMS, and dissolved after the final hydrogel structure is made**. B)** Colon carcinoma cell line, Caco-2 cells, was seeded onto the structure and cultured for 3 weeks until the whole structure was covered, forming finger-like structures mimicking the intestinal villi covered with epithelial

cells. Reproduced from [37] with permission from the Royal Society of Chemistry.

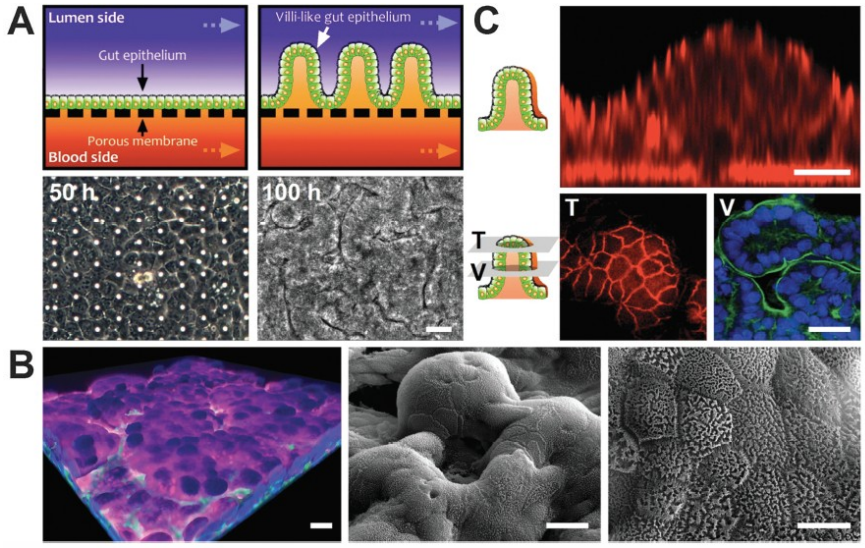

Figure 1.5: Formation of intestinal villi by CaCo-2 cells within in Gut-on-a-Chip cultures. (A) Schematic showing transformation of a planar intestinal epithelium into villus structure (top) and corresponding phase contrast images of CaCo-2 cells that undergo similar villus morphogenesis recorded at 50 and 100 h (bottom). **(B)** A 3D reconstruction of Z-stacked images of CaCo-2 villi stained for nuclei (blue), F-actin (green), and mucin 2 (magenta) is shown at the left. SEM images of these villi are shown at the middle and right at low and high magnification, respectively. **(C)** Schematics showing a vertical cross section and horizontal cross sections at the tip (T) versus middle (V) of a single villus are shown at the left. Immunofluorescence confocal viewsof CaCo-2 villi shown at the right demonstrate staining for the tight junction protein, ZO-1 (red) in vertical (top) versus horizontal en face sections of a CaCo-2 villus (bottom left). Bottom right view shows staining for the continuous apical brush border membrane labeled for F-actin (green) overlying the well oriented intestinal cell nuclei (blue). All scale bars are 25 mm, except right SEM image (scale bar, 10 mm). Reproduced from [42] with permission from the Royal Society of Chemistry.

1.3.2 *In vitro* 3D culture systems for drug delivery

In vitro test systems gain increasing importance in preclinical studies to increase the predictivity and reduce animal testing. Herein, barrier tissues are particularly interesting as they are the guards of human body. These barriers are formed by highly specialized tissues such as skin, lung,and gut. However, to recapitulate these tissues researchears are currently restricted by a lack of suitable models. Pharmaceuticals have to pass several preclinical studies in order to advance into clinical trials. Thee tests include *in vitro* and *in vivo* models to predict drug delivery, toxicity, and efficacy. Many drugs fail in the clinical studies due to poor bioavailability and nonspecific targeting, demonstrating the need for more predictive test systems. [42] Especially drug delivery is difficult to model in different species or cell culture models. The small intestine combines transport and barrier function within a simple columnar epithelium. [43]

In addition most substances have to pass the ECM, to enter in the blood stream. In addition, most substances have to pass the extracellular matrix to enter the bloodstream. While there is a wide array of *in vitro* or *ex vivo* tests available, most standard assays employ only simple 2D cell cultures. These test systems lack key features, such as polarization and differentiation of the barriers as well an extracellular matrix, leading to very low-barrier functions. It was shown that the matrix underlying the epithelium has a strong influence on the epithelium architecture and on the transport of substances. [44-45] Due to the low *in vitro-in vivo* correlation of many current models, these test systems are limited in their

predictions, which can lead to false results for drug delivery in the human body. [46] To address these pitfalls, tissue models containing a well differentiated and functional epithelium and a physiological scaffold are needed to create predictive 3D test systems. Through the advances in tissue engineering and material science, a broad variety of scaffolds mimicking the extracellular matrix have been introduced. Synthetic scaffolds such as porous polystyrene or polycarbonate membranes are easy to fabricate but lack physiological features. Collagen or matrigel hydrogels include the main proteins of the human tissue, but introduce some with disadvantages such as mechanical instability and contraction through fibroblast mediated remodeling. [47]

1.4 Nanomedicine and drug delivery: different carriers and approach

Nanomedicine and drug delivery have opened a new horizon of possibilities and strategies, particularly for controlled release and diagnostic. Drug delivery describes a process whereby a therapeutic agent is administrated to the body in a controlled manner. Drug delivery technologies make medicine more convenient and acceptable to a patient by simplyfing the dosing regimen and improving administration. [49]

During the last decades many nanocarriers have been realized. Everyone with an increasingly refined strategy.

More recently researcher focused on the development of "multifunctional" platforms, *i.e.* nano-vectors able to simultaneously or sequentially perform several functionalities:

- controlled degradation
- controlled drug release

Another important goalof this research activitiy, is the realization of a completely biocompatible and biodegradable nanocarrier. In particular, the main objective is the realization of nanometric sized drug vehicles, derived from natural materials, but holding the features needed for the drug delivery. In fact, the oil core carrier is built up with natural materials like soybean oil and egg lecithin and able to encapsulate hydrophobic drugs, like curcumin, paclitaxel, or some others benefical oils- like almond and bergamotto oils.

1.4.1 Monolayer deposition based on Layer by Layer technique

The layer-by-layer (LbL) deposition technique is a versatile approach for preparing nanoscale multimaterial films.
In particular, it is a versatile and robust technique for fabricating customized thin films of diverse composition. [50-52]
It provides a high level of control on properties such as thickness, composition and nanostructure. [53-54] The method has predominantly been used to assemble films using electrostatic 1-4 hydrogen-bonding [55-56] interactions or electrochemical deposition [57-58] and, recently, to fabricate polyelectrolyte multilayer capsules. [59] The latter ones have attracted widespread interest in the field of drug delivery due to their control in the preparation procedure and their multifunctional features. [57-61] In addition, polyelectrolytes are also emerging as bio-functional interfaces in tissue engineering.

[60] However, the main forces stabilizing LbL assembled systems are based on electrostatic interactions, making such systems very sensitive to environmental conditions, such as variations in the ionic strength or temperature of the medium, and thus susceptible to disassembly [61-62] which represents an important limitation for some biomedical applications.

1.4.2 O/W nanoemulsion

The development of nano-carriers capable of conveying and releasing bioactive substances is currently creating great interest and it is becoming one of the most important objectives of, above all, food, cosmetics and pharmaceutical industries. Oil-in-water (O/W) nano-emulsions, consisting of small lipid droplets dispersed in an aqueous medium, can besuitable as the basis of many kinds of foods (e.g., milk, cream, beverages, dressings, etc.), [63-64] as well as cosmetics (lotions, transparent milks, and crystal-clear gels). [62-65] Their ability to dissolve large quantities of hydrophobics and protect their cargo from hydrolysis and enzymatic degradation makes nano-emulsions ideal vehicles for the purpose of drug delivery. O/W nano-emulsions represent an ideal nano-carrier to conveying and releasing powerful poorly water-soluble drugs. [65-67] The covalently bound multilayer resulted to have an increased biostability, for both PS NPs and, more interestingly, O/W nano- emulsions templates. Moreover, the possibility to perform the cross- linkage without any photoinitiator, as demonstrated through cytotoxicity assays, and the choice of natural and biodegradable

components makes this approach highly biocompatible and efficient in the field of bio-applications.

1.4.3 Polysaccharides-based polyelectrolyte layers

Polysaccharides are natural polymers that belong to the family of the carbohydrates and play fundamental roles in many biological contexts. Their structure is made of sugar rings linked by glycosidic bonds and various side functions. These highly abundant molecules are from various origins including algal origin (e.g. alginate and carrageenan), plant origin (e.g. cellulose, pectin and guar gum), microbial origin (e.g. dextran and xanthan gum), and animal origin (e.g. chitosan, hyaluronan, chondroitin and heparin). Naturally occurring polysaccharides are diverse in their physicochemical properties. They possess multiple chemical structures (Figure 1.6) and the chemical composition greatly varies, as well as the molecular weight (Mw) and ionic nature. This versatility also contributes to a wide range of biological activities. From a pharmaceutical standpoint, polysaccharides possess many favourable characteristics such as low toxicity, biocompatibility, stability, low cost, hydrophilic nature and availability of reactive sites for chemical modification. Two elements are of utmost importance in the chemistry of polysaccharides. Firstly, the glycosidic bonds can be the target of glycoside hydrolase enzymes and can thus be biodegraded relatively easily. Secondly, the side groups can directly affect the polysaccharide charge density, hydration and chemical reactivity, and can also be responsible for the

formation of secondary structures. When charges are present, polysaccharides behave like polyelectrolytes. The negative groups (COO−) with pKa around 3–5 or sulfate groups (SO3−) with a pKa of around 0.5–1.5.32 The positively charged groups are ammonium groups ($NH3^{+}$) with a pKa of around 7–10.33, 34. In particular, the presence of negative and positive groups makes these polymers suitable for LbL application. [68] Indeed, Polyelectrolyte Multilayer (PEM) films give rise to self-assembly *via* LbL, because of both interactions between the negative and positive groups and the entropic gain associated with these interactions. In addition, the presence of carboxylic and ammonium group makes these polymers suitable for chemical modifications. However, certain difficulties are encountered when working with polysaccharides. Chemical modification can be a real challenge because of the high hydration shell and poor solubility in organic solvents.

Due to their lower solubility, pH and ionic strength can only be varied to a lower extent than for their synthetic counterparts. [69-70]

1.4.4 Chitosan modified Glycol Chitosan and thyolated glycol chitosan

Chitosan (CT) and glycol chitosan (GC) are linear polysaccharides composed of β-(1,4)-linked D-glucosamine and N-acetyl-D-glucosamine (Figure 1.6). Even though the discovery of chitosan dates from the 19th century, it has only been over the last three decades that this polymer has received attention as a material for biomedical and drug delivery applications. [68-72] The accumulated information about the physicochemical and biological properties of chitosan led to the recognition of this polymer as a promising material for drug delivery and, more specifically, for the delivery of delicate macromolecules. [73] CT is obtained by deacetylation from chitin, a highly abundant polysaccharide, which is the main component of the crustaceans and insect exoskeleton, and certain fungi. [74] Due to the limited solubility of chitin in aqueous solutions, chitosan is more suitable for industrial applications. [75] Whereas chitin is a polymer of N-acetyl-D-glucosamine units, chitosan is less easily defined in terms of its exact chemical composition. It usually refers to a family of polymers that are characterized by the number of sugar units per polymer molecule (n+m), which defines the molecular weight, and the degree of deacetylation (DD). The DD affects the pKa34 and, consequently, the solubility of chitosan in aqueous solutions, making the polymer soluble in acidic solutions and insoluble in neutral or in weak alkaline solutions. [76] The intriguing properties of CT have been known for many years and the polymer has been used in the fields of agriculture, industry and medicine. [77, 79] In particular, the

pharmaceutical and biomedical applications of CT probably offer the greatest promise. [78-81] CT lacks irritant or allergic effects and is biocompatible with both healthy and infected human skin.[80] When chitosan was administered orally in mice, the LD50 was found to be in excess of 16 g/kg, which is higher than that of sucrose. CT is approved for dietary applications in several country and it has been approved by the FDA for use in wound dressings.[82] Due to its protonable amine groups, CT has a polycationic nature and, therefore, is able to form PEM films. Actually, the choice of a polycationic polysaccharide is very limited. In fact, only chitosan is currently available and used in PEM films. [72] Due to its aforementioned numerous interesting properties, chitosan is probably by far the most widely used polysaccharide in LbL film.[71] Its positive charge also facilitates adhesion to mucosal surfaces, which are mostly negatively charged. [72] In addition, the amine groups can be also used for chemical modifications. The main problems concerning chemical modification of the amine group are (i) the difficulty to perform any modification with a limited pH working range and (ii) the reduced solubility of the modified chitosan in water due to the loss of free amine groups. Several attempts were made to improve the water solubility of CT, but most of them also reduce the fraction of free amine groups. On the other hand, a different modification of chitosan was proposed to obtain a polymer with improved water solubility but with no reduction of free amine groups. GC owes its water solubility to the incorporation of the hydrophilic glycol group, introduced by reacting chitin with ethylene oxide followed by its deacetylation. [75] For these reasons, GC could represent a valid alternative to CT for

the realization of PEM films, in particular when modified polymers are required. (Figure 1.7)

Another modification of chitosan with a thiolation agent, the N-acetyl-L-cysteine (NAC), through an amidation reaction with a water soluble carbodiimide as condensing agent (EDC, ethyl-3-(3-dimethylaminoisopropyl)-carbodiimide) and 1-hydroxy-1,2,3-benzotriazole (HOBt) as additive. (Figure 1.8)

Polymer characterization was performed with 1H NMR spectroscopy and the degree of functionalization was determined using the colorimetric Ellman's test.

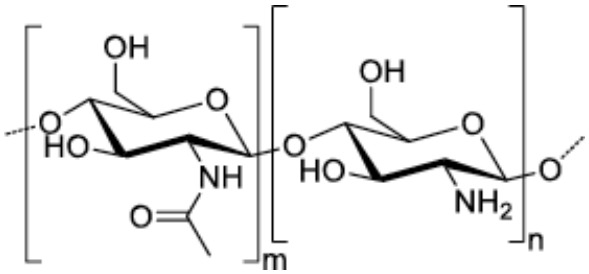

Figure 1.6. Chemical structure of chitosan. CT is a linear polysaccharide composed of β-(1,4)-linked D-glucosamine (n) and N-acetyl-D-glucosamine (m). The relative abundance of the acetylated or deacetylated forms can be expressed in percentage as Degree of Acetylation (DA) or Degree of Deacetylation (DD). The amine group of D-glucosamine results to be positively charged in acidic media making chitosan a polycation.

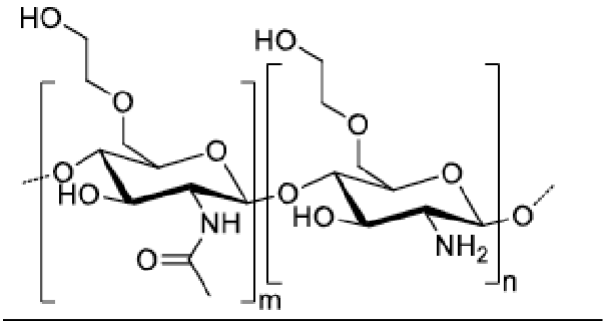

Figure 1.7. Chemical structure of glycol chitosan. GC is a modified chitosan with a glycol group linked to the hydroxyl in position 6 of the sugar ring.

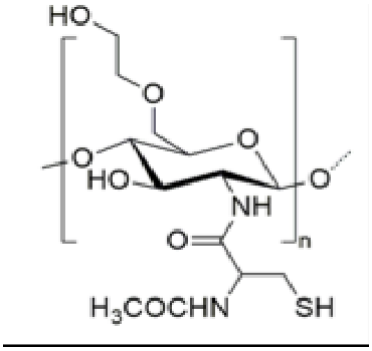

Figure 1.8. **Chemical structure of Thiolated Glycol Chitosan** (GC-NAC), is a modified glycol chitosan with the thiolated group on the deacitilated position.

1.5 Encapsulated nutraceuticals and drugs in O/W nanoemulsions

1.5.1 Curcumin

Curcumin is one of the two drugs of interest which have been investigated in my Phd thesis. It was encapsulated in an oil-in-water (O/W) nanoemulsion, for its poor stability. It is a natural component of the rhizome of turmeric (Curcuma longa) and one of the most powerful antiinflammatory agents. In many chronic illnesses in which inflammation plays a major role, curcumin has shown various therapeutic potentials such as anti -inflammatory and antioxidant properties. [84] Natural polyphenols have largely used for prevention and treatment of several disorders due to their antioxidant, anti-inflammatory effects. In contrast one of the main disavantages of their free administration is its low bioavailability. They show lipophilic nature and poor stability in aqueous solutions [85] resulting in low efficiency *via* oral administration. [86] Thus, different formulations were designed for the improvement of bioavailability of these compounds. [87-88]

Recently, we implemented a high performance nanocarrier system, capable of loading and protecting curcumin degradation. A selective coating on the nanoparticles enhances the bioavailability of curcumin.

1.5.2 Paclitaxel

The second drug explored in my thesis is paclitaxel (PXL). It is largely used as chemotherapic agent that has been used clinically for many years to treat ovarian, breast, lung, and pancreatic cancer. Recent studies showed the effects of PXL also in colon rectal cancer. The mechanism of action of PXL involves interference with the process of normal breakdown of microtubules during cell division, causing apoptosis in the treated cells. Furthermore, PXL acts as inhibitor in tumoral cells during glutaminolysis-related gene expression. [90-91] In the light of this, we tested the effect of encapsulated PXL on 3D tumoral systems and we evaluated its inhibiting properties.

1.12 References

[1] Tortora, G.J. and Nielsen, M.T., eds) (2012) Principles of Human Anatomy, John Wiley & Sons

[2] Marieb, E. et al. eds (2011) Human Anatomy, Pearson Benjamin Cummings

[3] Marsh, M.N. and Swift, J.A. (1969) A study of the small intestinal mucosa using the scanning electron microscope. Gut 10, 940–949

[4] Artis, D. (2008) Epithelial-cell recognition of commensal bacteria and maintenance of immune homeostasis in the gut. Nat. Rev. Immunol. 8, 411–420

[5] Mitic LL, Anderson JM. Molecular architecture of tight junctions. Annu Rev Physiol. 1998;60:121-42. Review. PubMed PMID: 9558457

[6] Amasheh S, Milatz S, Krug SM, Markov AG, Günzel D, Amasheh M, Fromm M. Tight junction proteins as channel formers and barrier builders. Ann N Y Acad Sci. 2009 May;1165:211-9. doi: 10.1111/j.1749-6632.2009.04439.x. PubMed PMID: 19538309.

[7] Dedhia PH, Bertaux-Skeirik N, Zavros Y, Spence JR: Organoid models of human gastrointestinal development and disease. Gastroenterology 2016, 150:1098-1112.)

[8] Artursson P, Lindmark T, Davis SS, Illum L. 1994. Effect of chitosan on the permeability of monolayers of intestinal epithelial cells (Caco-2). Pharmaceutical research 11(9):1358-1361.

[9] Karlsson J, Artursson P. 1991. A method for the determination of cellular permeability coefficients and aqueous boundary layer thickness in monolayers of intestinal epithelial (Caco-2) cells grown

in permeable filter chambers. International journal of pharmaceutics 71(1-2):55-64.

[10] Dedhia PH, Bertaux-Skeirik N, Zavros Y, Spence JR: Organoid models of human gastrointestinal development and disease. Gastroenterology 2016, 150:1098-1112.)

[11] F. Pampaloni, E. G. Reynaud, and E. H. K. Stelzer, "The third dimension bridges the gap between cell culture and live tissue," *Nat. Rev. Mol. Cell Biol.*, vol. 8, no. 10, pp. 839–845, Oct. 2007.

[12] M. J. Lysaght and A. L. Hazlehurst, "Tissue engineering: the end of the beginning," *Tissue Eng.*, vol. 10, no. 1–2, pp. 309–320, Feb. 2004.

[13] Ledford H. Translational research: 4 ways to fix the clinical trial. Nature 2011;477(7366):526-8. Doi:10.1038/477526a.

[14] Lullman-Rauch R. Histologie. 4 ed. Thieme ;2012

[15] Hutmacher DW, Goh JC, Teoh SH. An introduction to biodegrad- able materials for tissue engineering applications. Ann Acad Med Singap. 2001;30(2):183–91. [16]. Netti PA, Berk DA, Swartz MA, Grodzinsky AJ, Jain RK. Role of extracellular matrix assembly in interstitial transport in solid tu-mors.Cancer.Res.2000;60(9):2497–503.

[17]. Pusch J, Votteler M, Gohler S, Engl J, Hampel M, Walles H, et al The physiological performance of a three-dimensional model that mimics the microenvironment of the small intestine. Biomaterials. 2011;32(30):7469–78. doi:10.1016/j.biomaterials.2011.06.035.

[18]. Imamura Y, Mukohara T, Shimono Y, Funakoshi Y, Chayahara N, Toyoda M, *et al.* Comparison of 2D- and 3D-culture models as drug-testing platforms in breast cancer. Oncol Rep. 2015;33(4): 1837–43. doi:10.3892/or.2015.3767.

[19]. Ma L, Gao C, Mao Z, Zhou J, Shen J, Hu X, et al. Collagen/ chitosan porous scaffolds with improved biostability for skin tissue engineering. Biomaterials. 2003;24(26):4833–41.

[20] H. Fernandes, L. Moroni, C. van Blitterswijk, and J. de Boer, "Extracellular matrix and tissue engineering applications," *J. Mater. Chem.*, vol. 19, no. 31, p. 5474, 2009.

[21]S. Yang, K. F. Leong, Z. Du, and C. K. Chua, "The design of scaffolds for use in tissue engineering. Part I. Traditional factors," *Tissue Eng.*, vol. 7, no. 6, pp. 679–689, Dec. 2001.

[22] F. Rosso, G. Marino, A. Giordano, M. Barbarisi, D. Parmeggiani, and A. Barbarisi, "Smart materials as scaffolds for tissue engineering," *J. Cell. Physiol.*, vol. 203, no. 3, pp. 465–470, Jun. 2005.

[23] J. A. Hubbell, "Biomaterials in tissue engineering," *Biotechnol. Nat. Publ. Co.*, vol. 13, no. 6, pp. 565–576, Jun. 1995.

[24] R. Langer, J. P. Vacanti, C. A. Vacanti, A. Atala, L. E. Freed, and G. Vunjak-Novakovic, "Tissue Engineering: Biomedical Applications," *Tissue Eng.*, vol. 1, no. 2, pp. 151–161, Jun. 1995.

[25] R. M. Nerem and A. Sambanis, "Tissue Engineering: From Biology to Biological Substitutes," *Tissue Eng.*, vol. 1, no. 1, pp. 3–13, Mar. 1995.

[26] van de Kerkhof, E.G. et al. (2006) Innovative methods to study human intestinal drug metabolism in vitro: precision-cut slices compared with Ussing Chamber preparations. Drug Metab. Dispos. 34, 1893–1902

[27] Pusch, J. et al. (2011) The physiological performance of a three-dimensional model that mimics the microenvironment of the small intestine. Biomaterials 32, 7469–7478

[28] Mertsching H, Walles T, Hofmann M, Schanz J, Knapp WH. Engineering of a vascularized scaffold for artificial tissue and organ generation. Biomaterials. 2005;26(33):6610–7. doi:10.1016/j. biomaterials.2005.04.048.

[29] Groeber F, Engelhardt L, Lange J, Kurdyn S, Schmid FF, Rucker C, *et al*. A first vascularized skin equivalent for as an alternative to animal experimentation. ALTEX. 2016. doi:10.14573/altex.1604041.

[30] Steinke M, Dally I, Friedel G, Walles H, Walles T. Host-integration of a tissue-engineered airway patch: two-year follow-up in a single patient. Tissue Eng Part A. 2015;21(3–4):573–9. doi:10.1089/ten. TEA.2014.0200.

[31] Schweinlin *et al*: Human barrier models for the in vitro assessment of drug delivery. Drug Delivery and Transl. Res. 1336-016-0316-9

[32] Development of an advanced primary human *in vitro* model of the small intestine. Matthias Schweinlin1, Sabine Wilhelm1, Ivo Schwedhelm1, Jan Hansmann1, Rene Ritscher2, Christian Jurowich3, Heike Walles1,4, Marco Metzger1,4

[33] Totonelli, G. *et al*. (2012).A rat decellularized small bowel scaffold that preserves villus–crypt architecture for intestinal regeneration. Biomaterials 33, 3401–3410

[34] Wang, L. *et al.* (2009) Influence of micro-well biomimetic topography on intestinal epithelial Caco-2 cell phenotype.
Biomaterials 30, 6825–6834

[35] Wang, L. *et al.* (2010) Synergic effects of crypt-like topography and ECM proteins on intestinal cell behavior in collagen based membranes. Biomaterials 31, 7586–7598

[36] Lee, M. *et al.* (2005) Scaffold fabrication by indirect three-dimensional printing. Biomaterials 26, 4281–4289

[37] Sung, J.H. et al. (2011) Microscale 3-D hydrogel scaffold for biomimetic gastrointestinal (GI) tract model. Lab on a Chip 11, 389–392

[38] Leonard, F. *et al*. (2010) A three-dimensional coculture of enterocytes, monocytes and dendritic cells to model inflamed intestinal mucosa in vitro. Mol. Pharm. 7, 2103–2119

[39] Himes VB, Hu WS. Attachment and growth of mammalian cells on microcarriers with different ion exchange capacities. Biotechnol Bioeng. 1987 Jun;29(9):1155-63.

[40] Huang S, Deng T, Wang Y, Deng Z, He L, Liu S, et al. Multifunctional implantable particles for skin tissue regeneration: preparation, characterization, in vitro and in vivo studies. Acta Biomater. 2008 Jul;4(4):1057-66.

[42] Ingber et al 2013 Sep;5(9):1130-40. doi: 10.1039/c3ib40126j.

[43] Ledford H.Translational research : 4 ways to fix the clinical trial. Nature 2011;477 (7366):526-8

[44] F. Pampaloni The third dimension bridges the gap between cell culture and live tissue. Nat.Rev. Mol.Cell.Biol. Vol.8. no 10 pp 839-845, oct 2017

[45] Netti PA, Berk DA, swartz MA, Grodzinsky AJ, Jain RK. Role of extracellular matrix assembly in interstitial trasport in soldi tumor cancer. 2000

[46] M.J. Lysaght and A. L. Hazlehurst "Tissue engineering: the end of the beginning" TISSUE ENG. Vol 10 no 1-2 pp 309-320 feb 2004

[47]Lullman-Rauch R.Histologie. 4 ed. Thieme 2012

[48] R. P. Feynman, *Engineering and science*, 1960, 23, 22-36.
[49] I. Freestone, N. Meeks, M. Sax and C. Higgitt, *Gold Bulletin*, 2007, 40, 270-277.
[50] R. E. Smalley, 2001.
[51] Y. Ge, S. Li, S. Wang and R. Moore, *Nanomedicine: Principles and Perspectives*, Springer, 2014.
[52] A. Kumar, H. M. Mansour, A. Friedman and E. R. Blough, *Nanomedicine in drug delivery*, CRC Press, 2013.
[53] T. Cedervall, I. Lynch, S. Lindman, T. Berggård, E. Thulin, H. Nilsson, K. A. Dawson and S. Linse, *Proceedings of the National Academy of Sciences*, 2007, 104, 2050-2055.
[54] I. Lynch and K. A. Dawson, *Nano Today*, 2008, 3, 40-47.
[55] D. E. Owens and N. A. Peppas, *International journal of pharmaceutics*, 2006, 307, 93-102.
[56] A. L. Klibanov, K. Maruyama, V. P. Torchilin and L. Huang, *FEBS letters*, 1990, 268, 235-237.
[57] V. P. Torchilin and V. S. Trubetskoy, *Advanced drug delivery reviews*, 1995, 16, 141-155.
[58] Y. Matsumura and H. Maeda, *Cancer research*, 1986, 46, 6387-6392.
[59] D. Peer, J. M. Karp, S. Hong, O. C. Farokhzad, R. Margalit and R. Langer, *Nature nanotechnology*, 2007, 2, 751-760.
[60] J. Fang, H. Nakamura and H. Maeda, *Advanced drug delivery reviews*, 2011, 63, 136-151.
[61] V. Torchilin, *Advanced drug delivery reviews*, 2011, 63, 131-135.
[62] F. Alexis, E. Pridgen, L. K. Molnar and O. C. Farokhzad, *Molecular pharmaceutics*, 2008, 5, 505-515.

[63] V. P. Torchilin, in *Drug delivery*, Springer, 2010, pp. 3-53.
[64] L. Y. Qiu and Y. H. Bae, *Pharmaceutical research*, 2006, 23, 1-30.
[65] J. J. Richardson, M. Björnmalm and F. Caruso, *Science*, 2015, 348, 2491.
[66] J. Kirkland, *Analytical Chemistry*, 1965, 37, 1458-1461.
[67] R. Muzzarelli and C. Muzzarelli, in *Polysaccharides I*, Springer, 2005, pp. 151-209.
[68] M. Rinaudo, *Progress in polymer science*, 2006, 31, 603-632. 37
[69] R. A. Muzzarelli, C. Jeuniaux and G. W. Gooday, 1986.
[70] T. Crouzier, T. Boudou and C. Picart, *Current Opinion in Colloid & Interface Science*, 2010, 15, 417-426.
[71] C. Picart, A. Schneider, O. Etienne, J. Mutterer, P. Schaaf, C. Egles, N. Jessel and J.-C. Voegel, *Advanced Functional Materials*, 2005, 15, 1771-1780.
[72] Q. Z. Wang, X. G. Chen, N. Liu, S. X. Wang, C. S. Liu, X. H. Meng and C. G. Liu, *Carbohydrate polymers*, 2006, 65, 194-201.
[73] T. Crouzier, T. Boudou and C. Picart, *Current Opinion in Colloid & Interface Science*, 2010, 15, 417-426.
[74] K. Janes, P. Calvo and M. Alonso, *Advanced drug delivery reviews*, 2001, 47, 83-97.
[75] V. Dodane and V. D. Vilivalam, *Pharmaceutical Science & Technology Today*, 1998, 1, 246-253.
[76] S. Mima, M. Miya, R. Iwamoto and S. Yoshikawa, *Journal of Applied Polymer Science*, 1983, 28, 1909-1917.
[77] R. Muzzarelli and C. Muzzarelli, in *Polysaccharides I*, Springer, 2005, pp. 151-209.
[78] M. Rinaudo, *Progress in polymer science*, 2006, 31, 603-632. 37

[79] R. A. Muzzarelli, C. Jeuniaux and G. W. Gooday, 1986.
33. T. Kean and M. Thanou, *Advanced Drug Delivery Reviews*, 2010, 62, 3-11.
[80] E. Yilmaz, in *Biomaterials*, Springer, 2004, pp. 59-68.
[81] D. K. Knight, S. N. Shapka and B. G. Amsden, *Journal of Biomedical Materials Research Part A*, 2007, 83, 787-798.
[82] H. G. Garg, R. J. Linhardt and C. A. Hales, *Chemistry and biology of heparin and heparan sulfate*, Elsevier, 2011.
[83] R. J. Linhardt, *Journal of medicinal chemistry*, 2003, 46, 2551-
[79] R. J. Linhardt, S. A. Ampofo, J. Fareed, D. Hoppensteadt, J. Folkman and J. B. Mulliken, *Biochemistry*, 1992, 31, 12441-12445.
[84] S. Boddohi, C. E. Killingsworth and M. J. Kipper, *Biomacromolecules*, 2008, 9, 2021-2028.
[85] A. A. Antipov and G. B. Sukhorukov, *Advances in Colloid and Interface Science*, 2004, 111, 49-61. Aggarwal BB, Harikumar KB. 2009. Potential therapeutic effects of curcumin, the anti-inflammatory agent, against neurodegenerative, cardiovascular, pulmonary, metabolic, autoimmune and neoplastic diseases. The international journal of biochemistry & cell biology 41(1):40-59.
[86] Wang Y-J, Pan M-H, Cheng A-L, Lin L-I, Ho Y-S, Hsieh C-Y, Lin J-K. 1997. Stability of curcumin in buffer solutions and characterization of its degradation products. Journal of pharmaceutical and biomedical analysis 15(12):1867-1876.
[87] Basnet P, Skalko-Basnet N. 2011. Curcumin: an anti-inflammatory molecule from a curry spice on the path to cancer treatment. Molecules 16(6):4567-4598.

[88] Vecchione R, Ciotola U, Sagliano A, Bianchini P, Diaspro A, Netti P. 2014. Tunable stability of monodisperse secondary O/W nano-emulsions. Nanoscale 6(15):9300-9307.

[89] Saville M, Lietzau J, et al. Treatment of HIV-associated Kaposi's sarcoma with paclitaxel.Lancet 1995 26-28

[90] Ahmed AA, Wang X, Lu Z et al. Modulating microtubule stability enhances the cytotoxic response of cancer cells to paclitaxel.

[91] Mielgo A, Torres VA, Clair K, Barbero S, Stupack DG. Paclitaxel promotes a caspase 8-mediated apoptosis through death effector domain association with microtubules. *Oncogene*. 2009;28(40):3551–3562.

Chapter 2

"*In Vitro* Study of Intestinal Epithelial Interaction with Engineered Oil in Water Nanoemulsions Conveying Curcumin"

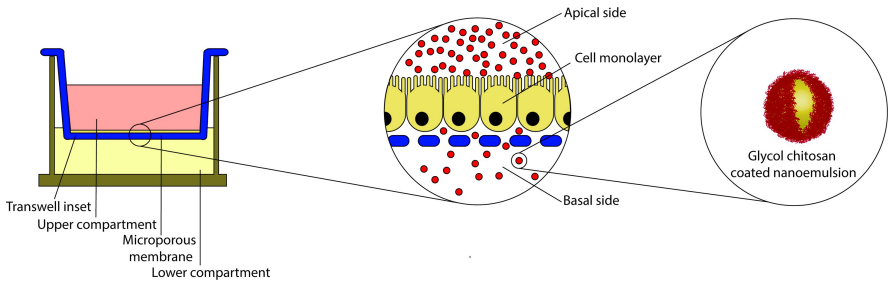

Adpted from Langella et al, 2017 "In vitro study of intestinal epithelial interaction with engineered oil in water nanoemulsions conveying curcumin", *submitted manuscript*.

Abstract

The development of innovative nano-bio-encapsulation systems continues to be an area of intense activity as the demand of improved delivery systems is constantly increasing in several fields including nanomedicine. For this purpose, an important goal is carrying out appropriate engineering of the surface of these nano-carriers to satisfy the organ target features for an effective *in situ* release and elucidate the mechanism of action which most of the time is neglected. Here, an oil-in-water (O/W) nanoemulsion coated with a polysaccharide layer film - *i.e.* a glycol chitosan modified with a thiol moiety - was used as nano-carrier to convey a powerful poorly water-soluble nature based drug, curcumin. The final nano-carrier was completely biocompatible and bio-stable. We investigated the enhancement of the effect of curcumin loaded in our system across monolayers of intestinal epithelial cells (CaCo-2) in transwell culture. Such *in vitro* platform resulted suitable to evaluate the functionality of the nano-carrier and its specificity towards the mucosal epithelial layer and, as applicative example, to investigate the anti-inflammatory effects exerted by the encapsulation of curcumin.

2.1 Introduction

The use of molecules or food ingredients with positive effects on health, prevention and treatment of diseases is increasingly in demand. [92] However, many nutraceuticals are unstable or poorly water soluble and their oral administration results to be limited. [93] The development of suitable carrier systems for oral delivery remains a major challenge for biomedical scientists and bioavailability remains limited even in the case of nano-encapsulation. As a consequence, oral formulations must be designed to preserve the drug from gastric absorption and improve its interaction with the intestinal tract.

An example of a powerful nutraceutical whose potentiality is not yet fully exploited is the curcumin. Among the naturally derived therapeutic products, curcumin, [1,7-Bis(4-hydroxy-3-methoxyphenyl)-hepta-1,6-diene-3,5-dione] is one of the most extensively studied in recent decades, due to its various properties. In many chronic illnesses in which inflammation plays a major role, curcumin has shown various therapeutic potentials such as anti-inflammatory and antioxidant properties. [94] In fact, molecular studies have indicated that curcumin blocks the activation of factors, such as cytokines, a class of enzymes present in human cells and able to trigger the inflammatory response. [95] Despite these attractive properties, curcumin has a very limited bioavailability because of its lipophilic nature and its poor stability in aqueous solutions [96] resulting in a low efficient oral administration. [97]

We recently proposed a high performance nanocarrier system, capable to load and protect curcumin from degradation and to enhance its bioavailability due to a coating with a thiol-modified chitosan. [98] It was demonstrated how important are the impact of some parameters such as size and degree of surface modification by direct evaluation of effects such as bioavailability, in *in vivo* anti-inflammation. However, while *in vivo* studies provide a direct proof of the validity of a drug delivery system, appropriate *in vitro* studies are necessary in order to specifically elucidate the mechanism of passage through the intestinal barrier. Nonetheless, there is an urgent need of highly fast, reliable and cost-effective *in vitro* models to predict intestinal absorption in order to reduce, refine or replace *in vivo* experimentation. [99] The intestine epithelial barrier is the first barrier and the most important location for the nutraceuticals coming from the lumen of the gut. The transport of drugs across the intestinal epithelium may occur by one, or more than one, of four different routes: the passive transcellular and paracellular routes, the carrier mediated route and by transcytosis. [100] Here, in order to comprehensively understand the route of the nano-system carrying the curcumin and the biochemical effect of the drug release, an air liquid interface (ALI) of CaCo-2 cells in transwell was effectively reproduced [101-104] and used as an *in vitro* testing platform. As previously reported, [105] the human CaCo-2 cells differentiate, after their polarization in culture, forming monolayers of mature intestinal enterocytes which can be used as a model that reproduce the intestinal barrier for *in vitro* prediction of intestinal drug absorption transport and toxicology studies. By using this model, we were able to demonstrate the interaction route and the biosafety of nanocarriers

in terms of cell viability and tight junction integrity as well as the curcumin bioavailability and its antioxidant effect on LPS-treated intestinal mucosa. Our results demonstrate that the proposed nano-carrier represents a very promising tool for the effective release of unstable and poorly water-soluble drugs.

2.2 Materials and methods

2.2.1 Materials

1-hydroxybenzotriazole hydrate (HOBt), n-acetyl-L-cysteine (NAC), Rhodamine B isothiocyanate (RBITC), paraformaldehyde and curcumin (from Curcuma Longa (Turmeric), powder, m.w. = 368.38 g/mol) were purchased from Sigma-Aldrich. Glycol chitosan was purchased from Wako Chemicals. 1-(3-dimethylaminopropyl)-3-ethyl-carbodiimide hydrochloride (EDC) was purchased from Iris Biotech. CaCo-2 cells were obtained from American Type Cell Culture (ATCC, Usa). Dulbecco's Modified Eagle's Medium (DMEM, Gibco, Life Technologies), supplemented with 10% fetal bovine Serum (FBS, Sigma Aldrich), 1% penicillin/streptomycin and 1% L-glutamine (Lonza, Milan) and 2% nonessential amino-acids NEEA (Euroclone, Milan). Hank's balanced salt solution (HBSS) was purchased from Gibco, Life Technologies. Transwell permeable supports (24-well plates with polyester membrane 0.4 μm) were purchased from Corning® Costar. FITC-Dextran was purchased from Molecular probes, Life Technologies. Trypsin was purchased from (Lonza). High Pure RNA tissue Kit was purchased from Roche. Transcriptor First Strand cDNA synthesis kit was purchased from Roche. SYBR® green master mix was purchased from Aurogene (2x SensiFaST SYBR). Primer of TNFα, TGFβ1, IL6 was purchased from Diatech. 3-(4,5-dimetiltiazol-2-thiazolyl)-2,5-difeniltetrazolio for MTT test, NMR solutions and LPS from Escherichia Coli were purchased from Sigma Aldrich.

2.2.2 Methods

2.2.2.1 Preparation of the nanocapsules

The nano-encapsulation system consists of an oil-in-water (O/W) nanoemulsion Vecchione *et al.* [98] coated with a mucoadhesive chitosan derivative, namely glycol chitosan. Glycol chitosan was opportunely modified with a thiol moiety (Figure 2.1). Oil in water nanoemulsion was obtained by using a high-pressure homogenizer (Microfluidics M110PS), as previously described Vecchione *et al.* [106] Briefly, 5.8 g of surfactant in 24 ml of oil were used and the oil phase was loaded with 100 mg of curcumin dissolved in 1 ml of ethanol. To promote dissolution, the oil phase containing surfactant and curcumin was mixed by alternating a high speed blender (RZR 2102 control, Heidolph) at 60 °C and 500 rpm to sonication with an immersion sonicator at room temperature (Ultrasonic Processor VCX500 Sonic and Materials), according to a process protocol previously reported Vecchione *et al.* [98] The curcumin loaded nanoemulsion was then coated with GC-NAC (glycol chitosan conjugated with N-acetylcysteine) or GC-RBITC-NAC (glycol chitosan conjugated with rhodamine B and N-acetylcysteine) by adding 1.5 ml of polymer solution (0.033 % (w/v) in acidified water at pH 4) to 1 ml of water suspensions of O/W nanoemulsion (5 % wt in acidified water at pH 4) under vigorous stirring. To perform the biological tests, a certain volume of sample was mixed with an equal volume of HBSS/DMEM (1:1) culture media, thus obtaining a final oil concentration of 1% (w/v) and a curcumin concentration in the O/W nanoemulsion is 0.42 mg/ml.

2.2.2.2 Modification of glycol chitosan with N-acetylcysteine (GC-NAC)

Glycol chitosan was modified with a thiol moiety, exploiting the EDC/HOBt chemistry, as previously described Calcagno *et al.* [107] Briefly, GC (100 mg, 0.20 mmol) was dissolved in 10 ml of Milli-Q water, HOBt (88,9 mg) was added and pH was at first adjusted to a value of 4 with HCl 1M to allow complete dissolution. Then, NAC (400 mg) and EDC (1,916 g) were added to the solution. The pH was adjusted and maintained to a value of 6.8. The reaction proceeded overnight at room temperature. The product was purified by dialysis four times against water containing 1 w/v% NaCl and acidified with HCl at pH=3 and four times against water acidified at pH=3. Finally, the purified product was freeze-dried for 48 h (Freeze dryer CHRIST Alpha 1-4 LSC). Free thiols were determined using a colorimetric assay, the Ellman's test. In particular, after reaction of thiolated chitosan with a DTNB solution at 25°C for 2 h, absorbance was registered at 412 nm using a Varian Cary Scan 100 Spectrophotometer. GC-RBITC-NAC was obtained with the same procedure, by using GC-RBITC instead of pristine GC.

2.2.2.3 Modification of glycol chitosan with rhodamine B isothiocyanate (GC-RBITC)

Glycol chitosan (100 mg, 0.20 mmol) was dissolved in 10 ml of 0.1 M of acetic acid solution. After complete dissolution, a solution of RBITC (7 mg in 700 µl of DMSO) was added dropwise. The reaction proceeded over night at room temperature. Sample was then dialyzed (dialysis tubing with a MWCO of 6-8 kDa) against water till no dye was detected (using Perkin Elmer 2300 Enspire plate reader, λ_{ex}= 555 nm, λ_{em}= 565 nm). Finally, the purified product was freeze-dried for 48 h.

2.2.2.4 LbL deposition of functionalized polymers on polystyrene carboxylated nanoparticles

Monolayer deposition. 1 ml of a water suspension (pH 4) of carboxyl latex beads (PS NPs, 0.5 % w/v) were added, under vigorous stirring for 15 min to 2 ml of a solution of GC (0.04 % w/v) in water at pH = 4.

2.2.2.5 Z-potential measurements

The Z-potential was determined using a particle electrophoresis instrument (Zetasizer zs nano series ZEN 3600, Malvern Instruments Ltd., Malvern, U.K.). Samples were diluted up to a concentration of

approximately 0.025 % w/v using the proper buffer solution. The Z-potential analysis was carried out by setting 50 runs for each measurement.

2.2.2.6 Particle size measurements

Suspensions were characterized using a laser dynamic light scattering (DLS) instrument (λ = 632.8 nm). A detecting angle of 173° was used. All the samples were diluted up to a droplet concentration of approximately 0.025 wt% by using Milli-Q water acidified at pH 4. A default refractive index ratio (1.5900) and 5 runs for each measurement (1 run lasting 100 s) were used in the calculations of the particle size distribution.

2.2.2.7 Modification of glycol chitosan with N-acetylcysteine (GC-NAC)

GC was modified with a thiol moiety, exploiting the EDC/HOBt chemistry, as previously described Calcagno *et al.* [107]. Briefly, GC (100 mg, 0.20 mmol) was dissolved in 10 ml of Milli-Q water, HOBt (88,9 mg) was added and pH was at first adjusted to a value of 4 with HCl 1M to allow complete dissolution. Then, NAC (400 mg) and EDC (1,916 g) were added to the solution. The pH was adjusted and maintained to a value of 6.8. The reaction proceeded overnight at room temperature. The product was purified by dialysis four times against water containing 1 w/v% NaCl and acidified with HCl at pH=3 and four times against water acidified at pH=3. Finally, the

purified product was freeze-dried for 48 h (Freeze dryer CHRIST Alpha 1-4 LSC). Free thiols were determined using a colorimetric assay, the Ellman's test. In particular, after reaction of thiolated chitosan with a DTNB solution at 25°C for 2 h, absorbance was registered at 412 nm using a Varian Cary Scan 100 Spectrophotometer. GC-RBITC_NAC was obtained with the same procedure, by using GC-RBITC instead of pristine GC.

2.2.2.8 Modification of GC with rhodamine B isothiocyanate (GC-RBITC)

GC (100 mg, 0.20 mmol) was dissolved in 10 ml of 0.1 M of acetic acid solution. After complete dissolution, a solution of RBITC (7 mg in 700 µl of DMSO) was added dropwise. The reaction proceeded over night at room temperature. Sample was then dialyzed (dialysis tubing with a MWCO of 6-8 kDa) against water till no dye was detected (using Perkin Elmer 2300 Enspire plate reader, λ_{ex}=555 nm, λ_{em}=565 nm). Finally, the purified (≅85%) product was freeze-dried for 48 h.

2.2.2.9 Cell lines and culture conditions

Human colonic epithelial cell line, CaCo-2 cells, were obtained from American Type Cell Culture (ATCC, USA) and were grown in Dulbecco's Modified Eagle's Medium (DMEM, Gibco) supplemented with Fetal Bovine Serum (FBS, Sigma Aldrich), 2 mM/l L-glutamine (Gibco), 100 IU/ml streptomycin/penicillin (Gibco) at 37°C with 5 % CO_2 in Transwell 24-well plates (6.5 mm

diameter, 0.4 μm pore polyester membrane insert). The cells were seeded at $1x10^5$ in 0.33 cm^2 and grown on polycarbonate membrane for two weeks. During the first week cells grows till to completely cover all the membrane surface, thus leading to a submerged layer; during the second week the upper medium is removed and cells are already capable to polarize, thus leading to an ALI. Medium was replaced every 2 days.

2.2.2.10 Electron microscopy

For the TEM analysis of nanocapsules, samples were first exposed to vapors of an OsO_4 water solution (1% wt) as oil core dopant for not less than 4 h then, about 10 μl of the sample were spread on a copper grid (200 mesh with carbon membrane). After carefully removing the excess of solution grids were left to dry overnight.). TEM images were obtained using a TECNAI 20 G2 (Thermo Fisher, Eindhoven) with a camera Eagle 2HS. The images were acquired at 200 KV; camera exposure time: 1 s; size 2048 x 2048. For SEM and Energy Dispersive X-ray Analysis (EDX) measurements a small drop of solution containing nanocapsules was spread onto the surface of an aluminum stub covered by a glass plate. The sample was then sputter-coated with a thin Pt/Pd or gold layer (10 nm) in a Cressington sputter coater 208HR. The aluminum stub containing the Pt/Pd or gold -coated sample was then placed in a FEG-SEM scanning electron microscope and imaged using 20 kV accelerating voltage. For imaging analysis of cells, samples were first fixed with a sodium cacodylate 0.1 M in glutaraldehyde solution (2.5% wt) at room temperature for 2 h. Sample was washed with a solution of 0.1 M

sodium cacodylate - 0.1 M sucrose (3 times in an ice bath for 10 min). Sample were then fixed with OsO_4 (1% wt. in 0.1 M sodium cacodylate - 0.1 M sucrose) and washed again with a solution of 0.1 M sodium cacodylate - 0.1 M sucrose (3 times in an ice bath for 10 min). In the end samples were dehydrated by replacing the water solution with a series of ethanol solutions (30%, 50%, 75%, 95%, 95%, 100%, 100%, 100% (v/v)) and dried with a Critical Point Drier (Leica EM CPD300). As for nanocapsules, the samples were then sputter-coated and imaged as previously described.

2.2.2.11 Cell cytotoxicity experiments

The cytotoxicity of the nano-emulsions was assessed on CaCo-2 cells using the MTT method according to the manufacturer's instructions (Dojindo Molecular Technologies Inc., Rockville, MD). Cells were seeded in 6-well plates at a density of 200000 cells per well in complete medium at 37 °C in a humidified 5% CO_2 atmosphere. The drug test was made with different concentration of curcumin-loaded nano-emulsions in oil (free drug, 1%, 2%, 5% 20%) and the viability was evaluated at different time points (2h, 4h, 6h, 8h, 12h, 24h, 48h 72h). At the end of the incubation period, cells were washed three times with PBS at pH 7.4 and incubated with 300 µl of a MTT solution (5 mg/ml in cell culture medium) for 4 h at 37 °C. In the end 150 µl of DMSO were added and samples were incubated for 1h at 37 °C. The absorbance measurements were acquired at 570 nm (Perkin Elmer 2300 Enspire plate reader, λ_{abs}=570 nm).

2.2.2.12 Confocal imaging

CaCo-*2* cell monolayers cultured in transwell were washed with PBS solution and fixed with paraformaldehyde 4% (v/v) at room temperature for 20 minutes. Permeabilization was performed by using a 0.01% Triton solution in PBS for 5 minutes, washing three times with PBS and incubating with specific staining. Actin filaments were stained with Phalloidin-Alexa Fluor® 488 conjugate (1:50 in PBS). Nuclei were stained with DRAQ5™ (1:10000 in PBS). Cellular morphology of the CaCo-2 cells was observed with a Leica SP5 II laser scanning confocal microscope using a 63X oil immersion objective (HCX PL APO CS 63.0x1.40 OIL UV). Samples were observed with the following specific fluorescence channels: cytoskeleton (Phalloidin-Alexa Fluor® 488) λ_{ex}=488 nm (Argon Laser) and λ_{em}=500-530 nm, nanoemulsions coated with GC-RBITC-NAC (rhodamine B) λ_{ex}=543 nm (Helium Laser) λ_{em}=560-610 nm; nuclei (DRAQ5™) λ_{ex}=633 nm λ_{em}=650-750 nm. Z-Stack and Y-Stack image series were acquired to study the localization of labeled-drug in the CaCo-2 cells. Section thickness was set to 0.7 µm for all the images. Images analysis were performed using Fiji (Image J, plugin) and LAS AF (Leica Applications System).

2.2.2.13 Confocal analysis of CLN

Samples containing curcumin loaded nanoemulsions coated with GC-RBITC-NAC were opportunely diluted with HBSS/DMEM buffer and 200 µl were put in a FD3510 dish (WPI, Germany) for 30 min to

allow it to adhere to the glass surface. Sample in excess was washed twice by replacing it with 130 µl of HBSS/DMEM solution every 10 minutes and, in the end, with 130 µl of 5% (w/v) DABCO anti-fade solution (needed to avoid the bleaching effect of the Rhodamine B). For this analysis we used the same parameters used for cells.

2.2.2.14 Transepithelial Electrical Resistance assay

Transepithelial Electrical Resistance (TEER) of CaCo-2 epithelium-equivalent cultured in transwell was measured by using the Millicell-ERS (Electrical Resistence System, Millipore Corporation). The measured value was multiplied by the area of the membrane (1.12 cm^2) in transwell insert to obtain a TEER value expressed in Ohm x cm^2 and blank subtracted in order to evaluate the cell monolayer integrity during permeation experiments. TEER test was carried out to examine the ability of CLN based on glycol thiolated chitosan (GCNAC) on the opening of the tight junctions at predetermined time intervals of 0h, 3h and 24 h. The experiments were done in triplicate.

2.2.2.15 Immunofluorescence assay

Tight junctions of the CaCo-2 epithelium-equivalent *cultured* in *Transwell* were stained using a primary antibody (ZO-1). Cells were washed with PBS solution and fixed with paraformaldehyde 4% (v/v) at room temperature for 20 minutes.

Permeabilization was performed using a 0.01% Triton solution in PBS for 10 minutes, washing three times with PBS and first incubating with a blocking solution (PBS, BSA 5% and Triton 0.01%) for 2 h in a wet chamber. After washing with PBS, cells were incubated with ZO-1 antibody (1:50 in PBS) overnight at 4°C. Finally, cytoskeleton and nuclei were stained with Phalloidin-Alexa Fluor® 488 and DRAQ5™ solutions, as previously reported.

2.2.2.16 Apical-to-basal permeability assay

The permeability of CaCo-2 epithelium-equivalent cultured *i*n transwell was performed by measuring in dynamic and static conditions the trans-epithelial passage of the O/W nanoemulsion coated with GC-RBITC-NAC, of a blank sample (HBSS/DMEM, 1:1) and of FITC-Dextran solution (1 mg/ml diluted 1:100 in HBSS), generally used as positive control. Cells monolayers were incubated for 24 h at 37°C with 5 % CO_2; for dynamic condition a rotator at 80 rpm was used. A certain volume of HBSS/DMEM (1:1 V/V) was placed in the basolateral chamber in order to guarantee the dipping of the lower side of the membrane. The passage was determined by confocal imaging (Leica SP5 II Laser Scanning Confocal Microscope) and fluorescence emission of rhodamine and fluorescein, respectively (Perkin Elmer 2300 Enspire plate reader λ_{ex}=555 nm, λ_{em}=565 nm and).

2.2.2.17 Collection and NMR Analysis of Supernatants

After 3 h incubation of Caco2 cells with CLN, supernatants and cells were collected and the presence of curcumin was analyzed by Nuclear Magnetic Resonance (NMR). NMR was performed using an Agilent 600 MHz (14 T) spectrometer equipped with a DD2 console and a OneNMR HX probe. NMR spectra were recorded with a total of 256 transients and a PRESAT sequence was used to saturate the water residual peak. Spectra analysis was performed using VNMR*J* 4.0 software.

2.2.2.18 LPS induction

Caco-2 cells were treated with a Lipopolysaccharide (LPS) solution (5 μg/mL) for 3 hours to induce an inflammatory response, thus stimulating the overexpression of pro-inflammatory cytokines like TNFα, IL-6 and reducing the expression of $TGF\beta_1$. After the inflammatory induction, epithelial cells were treated with nano-emulsions to evaluate the anti-inflammatory effects of curcumin.

2.2.2.19 RT-PCR

Total RNA was extracted using High Pure RNA (Roche), according to the manufacturer's instruction. Synthesis of cDNA was performed using Kit iScript supermix according to the manufacturer's instruction. Analysis of mRNA expression was determined with quantitative real-time PCR using 2x SensiFaST SYBR, Bioline,

Aurogene, 1.2 μmol primers of GAPDH as a housekeeping gene for normalization and 1.2 μmol primers of TNFα, IL6 pro-inflammatory genes and TGFβ_1 anti-inflammatory gene, according to the manufacturer's instruction. Sequences of primers for GAPDH: Primer forward: 5'-CGGAGTCAACGGATTTGGTCGTAT-3'and reverse: 3'-AGCCTTCTCCATGGTGGTGAAGAC-5'; TNFα forward 5'-AAAGTAGACCTGCCCAGACTCGG-3' and reverse 5'-GAGCACTGAAAGCATGATCCG-3'; IL-6 Primer forward: TCTCCACAAGCGCCTTCGGT and reverse: TGGGGCAGGGAAGGCAGC; TGF β_1 forward 5'-CCGACTACTACGCCAAGGAGGTCAC-3' and reverse 5'-AGGCCGGTTCATGCCATGAATGGTG-3'. The relative fold change in gene expression was quantified using the $2^{-\Delta\Delta CT}$ method by normalizing the target gene expression to GAPDH and relative to the expression on the experimental control sample, as indicated in Figure 7. Data are the means ± SD of triplicate samples of at least two independent experiments. Student's t-test was used to determine statistical differences between mean values, and $P < 0.01$ was considered to be a significant difference.

2.3 Results and Discussions

2.3.1 CLN formulation and analysis

The presented nanocapsules consist of an oil core and a hydrophilic shell based on a glycol thiolated chitosan interface (Figure 2.1). The lipophilic nature of the oil core nanocapsules enables to load high amounts of lipophilic drugs, nutraceuticals like curcumin, dyes or contrasting agents. Due to the negative charge, the so realized oil core results suitable for the deposition of one or more polyelectrolyte layers by exploiting the LbL technique. Vecchione *et al* [98] In particular, we coated the nanoemulsion with a thiol modified glycol chitosan. Recently it was showed that chitosan modified with thiol groups determines an enhanced mucoadhesion due to the covalent bound with the cysteine residues of the mucus glycoproteins. This condition improves the permeability of epithelial-like constructs produced with CaCo-2 cells as proved by TEER reduction. [106, 107] Here, such thiolated glycol chitosan was used as coating for the curcumin loaded nanoemulsion (CLN). This is in agreement to the observations reported in the final part of this chapter (Supplementary results). Curcumin was chosen as model drug because of its lipophilic nature, its poor stability and its poor oral administration. [108] Curcumin was loaded at a concentration of 0,42 mg/ml of oil. Compared to the starting O/W nanoemulsion loaded with curcumin (105.1 nm and PDI = 0.060), the size of the same nanoemulsion coated with thiolated glycol chitosan, increased of only few nanometers (106.1 nm) and the PDI value remained below 0.1

(~0.08) (see Figure 2.2). The chitosan derivative was labelled with a fluorophore, rhodamine-B, which allowed to acquire confocal images of CLN (Figure 2.1A).

Electron microscopy imaging of CLN (Figure 2.1B and 2.1C), with OsO_4 stained oil assessed a narrow size distribution and nanocapsules size of around 100 nm.

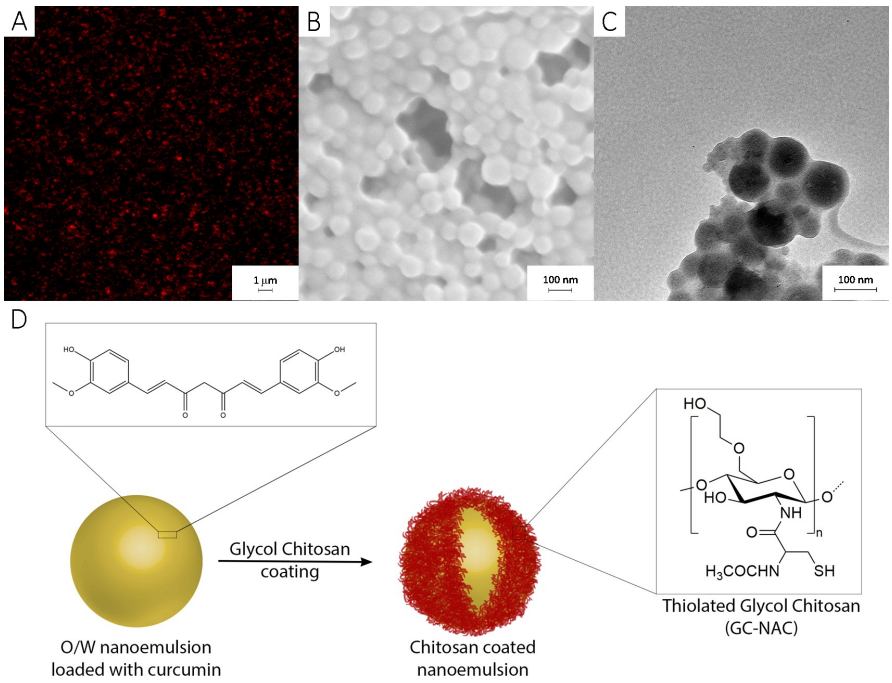

Figure 2.1: A) Imaging characterization of O/W nanoemulsion coated with GC-RBITC-NAC. B) Confocal image of CLN coated with rhodamine B labeled glycol chitosan; C) SEM image and D) TEM image of CLN stained with OsO_4 vapors. Osmium staining strengthened the soft CLN in order to avoid collapse due to the vacuum of electron microscopes.
Adapted from [124].

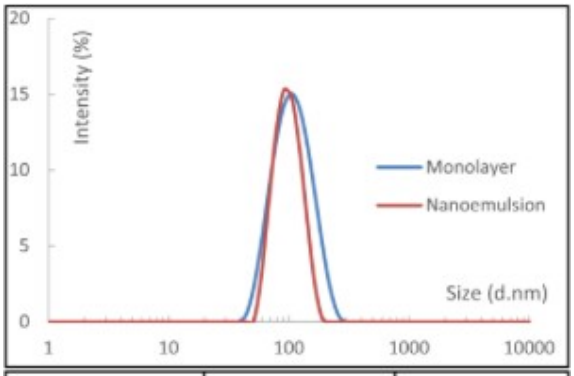

	Size (d.nm)	PDI
LNC	105.1	0.060
Monolayer GCNAC 1%	106.3	0.073

Figure 2.2: DLS analysis of free nanoemulsion (blue line) and monolayer GCNAC 1% (orange line).
Adapted from [124].

2.3.2 *In vitro* ALI model to test curcumin loaded nanocapsules

Intestine epithelium model produced by culturing CaCo2 cells in ALI was used as in *vitro* testing platform to evaluate safety, interaction and anti-inflammatory activity of the proposed curcumin loaded nanocapsules (Figure 2.3).

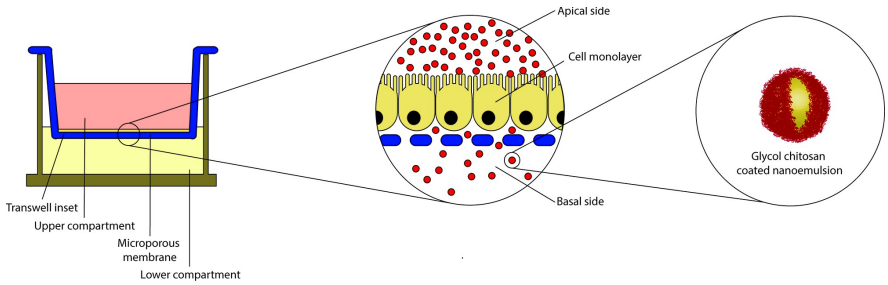

Figure 2.3: schematic representation of air liquid interface of CaCo-2 equivalent epithelium in Transwell system (on the left). In the central insert an enlarged view of the cell monolayer grown on the microporous membrane. On the right the oral nano-delivery system consisting of O/W nanoemulsion coated with a thiolayed glycol chitosan.
Adapted from [124].

We tested the biosafety of the CLN by carrying out cytotoxicity tests on CaCo-2 epithelium-equivalent by means of MTT test. The tested CLN did not induce significant suppression on the CaCo-2 cell viability as shown in Figure 2.4A. Moreover, the MTT data were confirmed by the ultrastructural analysis of polarized CaCo-2 epithelium-equivalent that shows preservation of nuclei, mitochondrial integrity and polarization of CaCo-2 that formed actin-based brush border structures (Figure 2.4B and 2.4C).

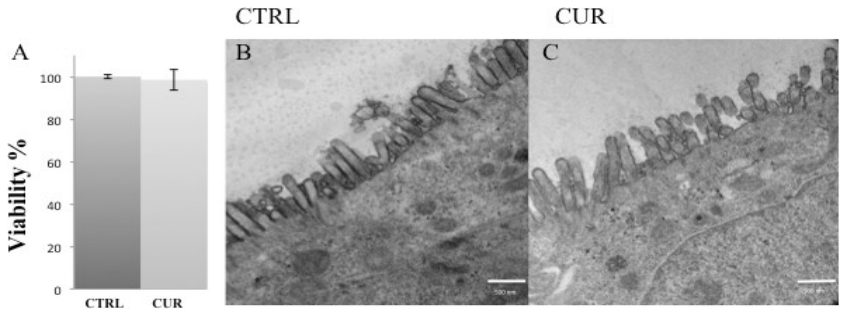

Figure 2.4: Cell viability. **MTT** This graph shows the cell viability after nanoemulsion treatment. **A)** Untreated Control and **B)** treated with CLN (GC-RBITC-NAC). Ultrastructural analysis of CaCo2 epithelium-equivalent at trasmission electron microscopy (TEM) B) untreated and **C)** cur treated, shows that nuclei are preserved, mithocondrial morphology is conserved, polarization of microvillus is manteined in both images.
Adapted from [124].

It is known that chitosan crosses the membrane by choosing the paracellular route. For this purpose, we performed TEER analysis to quantitatively measure the effects of the interaction mechanisms in terms of reversible opening of the intestinal tight junctions. [106, 109-111] Low molecular weight FITC-dextran was used as a positive control to monitor the paracellular transport across intestinal epithelial barrier (data not shown) confirming that the CaCo-2 epithelium-equivalent represents a functional model for the prediction of passive paracellular transport and for the study of drug absorption. [112] Chitosan's tight junction-opening effect induced a reduction of TEER (19%) and consequent permeability enhancement, between the start time point t = 0 h (~733,6 ohm*cm^2) and the end time point t = 3 h (~595,9 ohm*cm^2). The high degree of TEER reversibility suggests neither cell damage nor cell layer integrity loss confirming that the tight junctions opening induced by the proposed CLN were reversible. The integrity of tight junctions was further confirmed by immunofluorescence analysis for ZO-1. In figure 2.5 A-B, ZO-1 was correctly localized at intercellular level in the CaCo-2 epithelium-equivalent as in the case of the control.

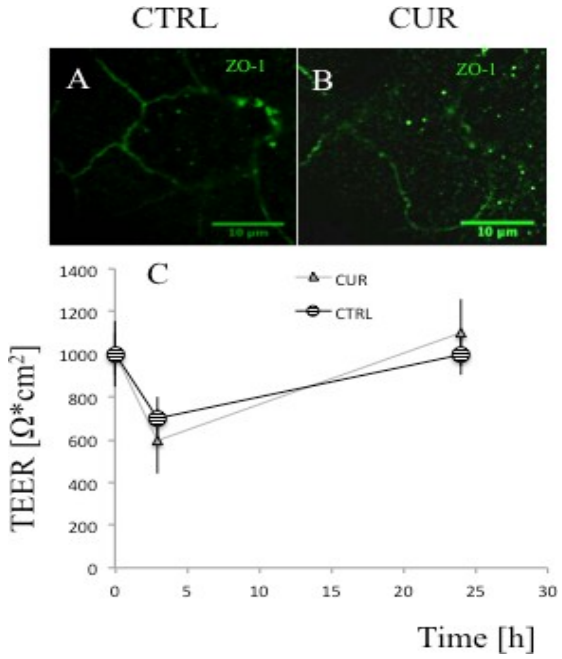

Figure *2*.5: Barrier functionality of epithelial monolayer of CaCo-2 cells:

Confocal images of Untreated Control 3h (a-b) and 3h treated with CLN (GC-RBITC-NAC) . This images showed a qualitative variation of permeability after 3 h of exposure to CLN; the effect is expressed by zo-1 staining.

Quantitative evaluation of (C) TEER on CaCo2 epithelium-equivalent showed a variation of permeability at time point 0h , 3h and .24h after rinsing the monolayer with HBSS-DMEM on the monolayer. Data are expressed as means ± SD of three experiments. Adapted from [124].

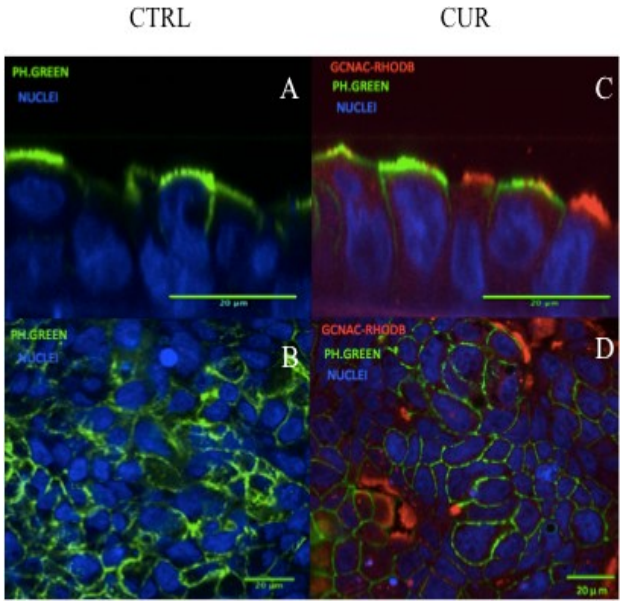

Figure 2.6: Confocal images of CaCo2 epithelium-equivalent: A-C) Y-view matching on the left ctrl and on the right 3h treated samples with CLN (GCNACRITCB) and B-D) on the bottom Z-view matching on the left control and on the right 3 h treated sample with CLN (GCNACRITCB). Adapted from [124]

Furthermore, confocal imaging was used to qualitatively visualize the transport and localization of CLN. In Figure2.6 we showed the Y and Z sections of CaCo-2 equivalent epithelium acquired with confocal microscope. GC coating was covalently labelled with Rhodamine B. This labelling, together with the specific staining of the biological

sample, allowed to discriminate among CLN (red channel), cell nuclei (blue channel) and cell cytoskeleton (green channel). Confocal analysis highlighted the presence, the localization and the transport of the proposed CLN. We demonstrated that, after 3 h, CLN was distributed on the surface of CaCo-2 equivalent epithelium, probably due to the ionic interaction between chitosan and mucus layer (Figure 2.6C-D). Indeed, the CLN appeared to be retained within the enterocytes as showed by the red signal located within the cells (Figure 2.6C-D). Hence, it can be noticed that also a transcellular route was chosen by the CLN.

2.3.3 NMR analysis of supernatants and cells:

The presence of curcumin above, inside and below the intestinal epithelia was evaluated by NMR (Figure 2.7). An NMR analysis was performed to evaluate curcumin in the upper and lower compartment of the *in vitro* model as well as inside the intestinal epithelia. In particular, in figure 2.7, we show the NMR spectra of CLN with no incubation (TQ 0 h), CLN after 3 h incubation on CaCo-2 cells (Upper 3 h), CaCo-2 cells after the same incubation time with CLN (Cell 3 h), basal compartment composed by HBSS:DMEM 1:1 and CLN that have crossed the intestinal barrier again after 3 h incubation (Lower 3 h). Spectra region between 7.3 ppm and 6.7 ppm contains peaks relatives to the aromatic protons of curcumin. Therefore, comparing the spectra of TQ, upper, cell and lower samples after 3 h of treatment, it is clear that curcumin decreases in upper part and increases in both cell and lower samples. It can be also noticed that the total amount of curcumin is strongly reduced in the upper solution

after 3 h of incubation, due to the adsorption and crossing of the cells monolayer.

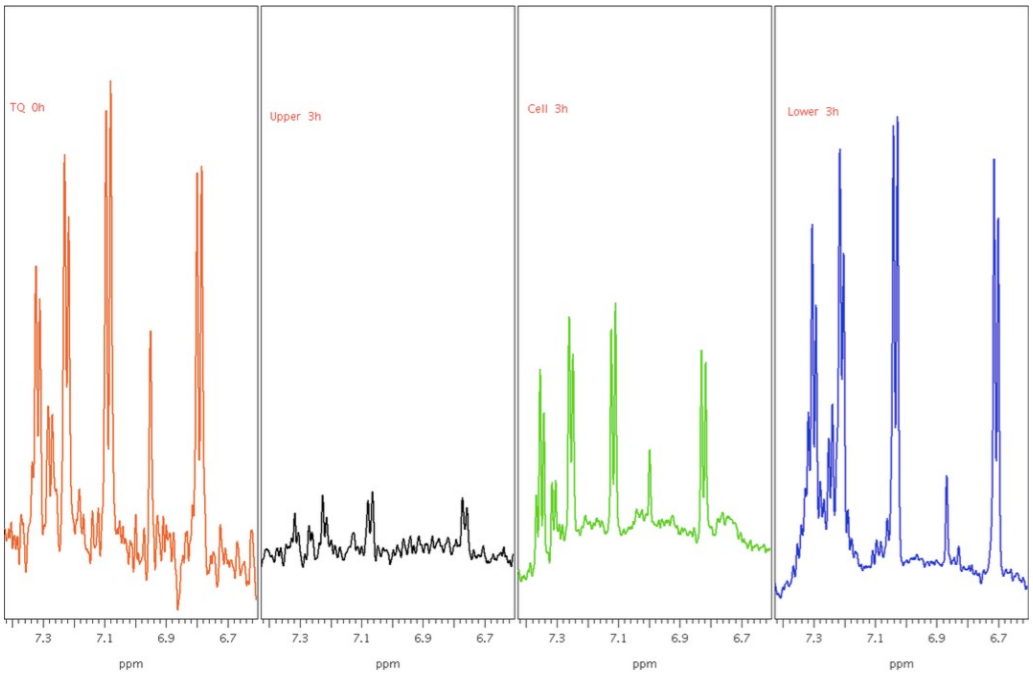

Figure 2.7. Aromatic region zoom from NMR spectra of CLN (TQ 0 h), CLN after 3 h incubation on CaCo-2 cells (Upper 3 h), CaCo-2 cells after 3 h incubation with CLN (Cell 3 h), basal compartment composed by hbss:dmem 1:1 and CLN that have crossed the intestinal barrier after 3 h incubation (Lower 3 h) Adapted from [124].

2.3.4 Molecular effects: evaluation of the expression of anti-inflammatory and proinflammatory genes after curcumine treatment:

In order to confirm the CLN release within the CaCo-2 equivalent epithelium we also evaluated their anti-inflammatory effect. As broadly reported in literature, curcumin is able to suppress inflammation via multiple pathways [95, 113,114] such as inhibiting the expression of various pro-inflammatory cytokines (e.g., TNFα, IL6, etc.) and increasing the anti-inflammatory cytokines (TGFβ1). To determine whether the CLN treatment could affect the inflammatory state of the CaCo-2 epithelium-equivalent, their gene expression of pro- and anti- inflammatory cytokines (TNFα, IL-6 and TGFβ1) was analyzed by RT-PCR. It is well known that TNFα plays a crucial role during acute inflammation with a wide range of intracellular signaling event [115]. Furthermore, TNFα activate several cytokines, such as IL-1b, IL-6 and IL-8 that have a role of amplify the inflammatory response which results in intestinal injury [116]. In our study, TNFα and IL-6 mRNA levels were significantly upregulated after LPS induction, showing that the inflammation model was successfully established. Several studies have demonstrated that LPS-stimulated CaCo-2 strongly increases the TNFα, IL-1b, IL-6 and IL-8 expressions in intestinal inflamed tissue

model [117]. In terms of the immunomodulatory action, it was interesting to note that in our model CLN had an effect on the LPS-induced TNFα secretion by CaCo-2 cells. Hence, TNFα and IL-6 gene expression was downregulated in LPS-stimulated CaCo-2 treated with CLN (Figure 2.8 a and 2.8b) compared with the control (untreated cells). It was also found that gene expression of TGFβ1, another central cytokines that plays a critical role in the inflammatory response [118], was up-regulated in LPS-stimulated CaCo-2 treated with CLN compared with that of the untreated cells. No significant differences of either the IL-8 and IL-10 mRNA level existed between those two groups, because a relatively higher expression level of gene was observed in the untreated culture (data not shown). These results provide further evidence that proposed CLN significantly contribute to reduce the inflammatory state in LPS-stimulated CaCo-2 cells. Based on these results, it can be assumed that the use of a modified chitosan as external interface of our CLN was a very good strategy to carry selectively the curcumin between and within the cells.

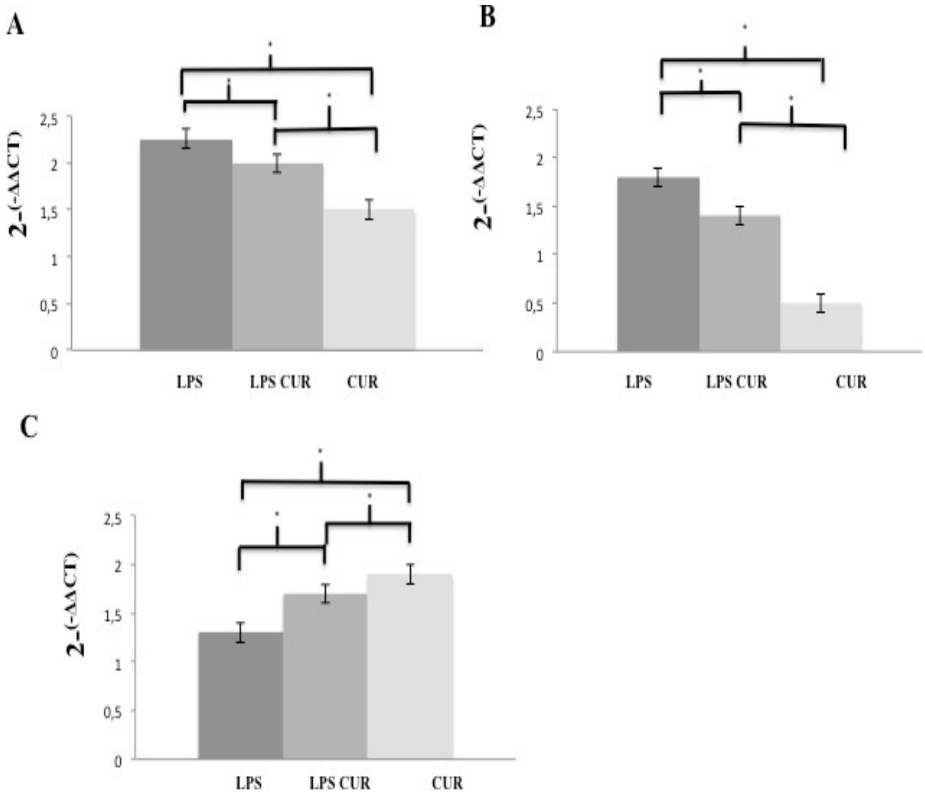

Figure 2.8: Molecular effects via q-PCR of differentes cytokines: (a) Pro-inflammatory effect of TNFα, (B) IL6 before and after CLN treatment in a LPS induced cells. (C) Anti-inflammatory effect of T GFβ1 before and after CLN treatment in a LPS induced cells. Data are expressed as means ± SD of three experiments. All samples have a p- value (< 0.01) Adapted from [124].

2.4 Conclusions

The beneficial properties of curcumin could play an important role for the treatment and the prevention of different inflammatory diseases. Main limitation of lipophilic molecules, like curcumin, is related to their low bioavailability. For this purpose, up to now a plethora of nanocarriers for the transport of curcumin or other lipophilic natural compounds have been proposed.

In this study, we used a nanocarrier based on an oil in water nanoemulsion to convey curcumin by keeping its anti-inflammatory activity and we studied this nanocarrier from different points of view. In particular, we assess a favorable interaction of the nanoemulsion with an advanced air liquid interface (ALI) model of the intestinal barrier without any damage of the same. Moreover, the anti-inflammatory effects were investigated and proved, thus demonstrating that this formulation can effectively protect the drug from degradation. These results show the promising use of the proposed nanocapsules for the oral delivery of lipophilic and sensitive drugs like curcumin.

2.5 Supporting results

2.5.1 Functionalized polystyrene nanoparticles as a model before O/W nanoemulsion particles for studying bio-nanointeractions

2.5.2 Polymer functionalizations (GC) and (GC-NAC)

We used polystyrenes nanoparticles (Nps) coated with GC and GC-NAC to evaluate how the two kinds of chitosan can affect uptake and distribution of the nanocarriers in different *in vitro* models.

We chose polystyrene as a material, being non-degradable in the cellular environment and for its comproved non-toxicity to cells.

Polymer functionalization is one of the best strategies to be taken for drug delivery on the target organ. The choice of chitosan as a polymer allows a lot of modifications, due to its structure described in the preview chapter. GC is a water-soluble chitosan and improves the crossing of epithelial tissue.

Mucoadhesion concept came out in the early's 80's by Professor J.R Robinson at the Wisconsin University that introduced the concept of "mucoadhesion" as a new route to prolong the residence time of drugs on the ocular surface. During the time other mucosal

membranes have proved to be favorable to mucoadhesive polymers. For istance, a lot of mucoadhesive polymers were exploited for targeting a drug to particularly region of the body for prolonged period of time [119].

Recently, it was shown that chitosan modified with thiol groups determines an enhanced mucoadhesion due to the covalent bound with the cysteine residues of the mucus glycoproteins.

2.5.3 *In vitro* distribution of functionalized polystyrene nanoparticles with glycol chitosan and thiolated glycol chitosan

CaCo-2 cells seeded in transwell after one week of Air Liquid Interface (ALI) was used as *in vitro* testing platform to evaluate the differences in terms of crossing or distribution on intestinal cells, between glycol chitosan (GC) and thiolated glycol chitosan (GCNAC).

As mentioned earlier, the substantial difference between the first and the second chitosan modification is that of crossing and remaning on the epithelial surface due to the presence of thiols that interacts with the presence of some mucus residues. We have evaluated the permeability of these two modified chitosan with (TEER) measurements and due to the presence of rhodamine B we have evaluated the distribution of NPS on cells by confocal analysis.

2.5.4 TEER measurements

TEER of CaCo-2 was evaluated before and after 3 h and 24 h treatment in order to evaluate the temporary degree of TEER (Figure 2.2.1). In fact, after 24 h tight junctions come back in the initial conditions. In fact, results showed in figure 2.2.1 suggest that TEER decreases in both GC and GCNAC. However, in the case of GC TEER value in average is the lowest. Thus, the first polymer (GC) is more permeable and water soluble so is more likely to cross the membrane. GCNAC stays more on the epithelial surface due to the disulphide bond with the thiols at the mucus cellular residues.

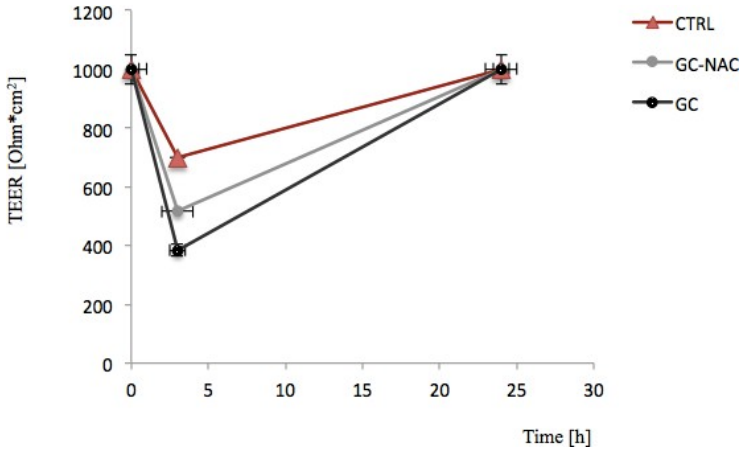

Figure 2.2.1: Transepithelial Electrical Reistence of Caco-2 before and after treatment with glycol chitosan (GC) and thiolated glycol chitosan (GCNAC). Measurement of TEER suggest that glycol chitosan is able to reduce more TEER value for its high solubility and permeability while thiolated chitosan that reduces the TEER value less, maybe because its mucoadhesion properties.

2.5.5 Confocal analysis

In order to distinguish between two different kinds of chitosan, namely glycol chitosan (GC) and (GCNAC) modified glycol chitosan, by labeling the two polymers with a fluorophore it was possible to make confocal comparisons.

In Figure 2.2.2 and 2.2.3, following the rhodamine tag (red signal) on the nanocapsules, it was possible to observe the different distribution both outside and inside the cells (nuclei in blue) associated to the two different chitosans. In Figure 2.2.2 polystirene nanoparticles coated with NAC modified glycol chitosan were distribuited mainly on the cell monolayer due to the strong interaction with disulphide bonds. Conversely, in Figure 2.2.3 it is shown a deep penetration of the polymers and therefore of the nanocarries in the tissue.

Thus, these results explain the final route chosen by nanocarriers depending on the different chitosan.

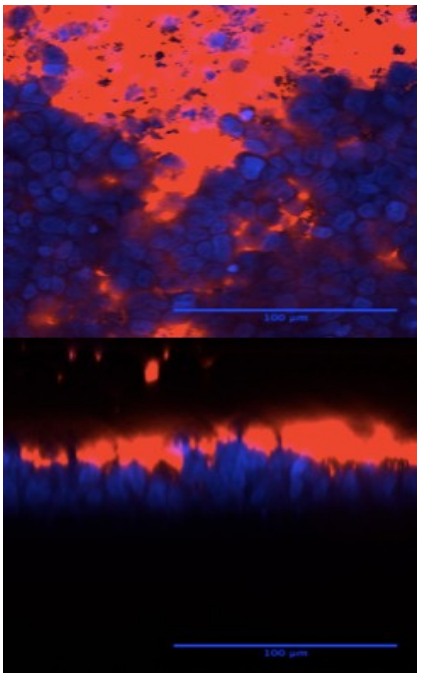

Figure2.2.2. GCNAC on CaCo-2 cells.
In this figure the distribution of the polymer elucidate the mucoadhesive properties of the chitosan on CaCo-2 equivalent intestinal epithelium. In Z and in Y-view the polymer remains on the surface principally and pass gradually across the cell monolayer.

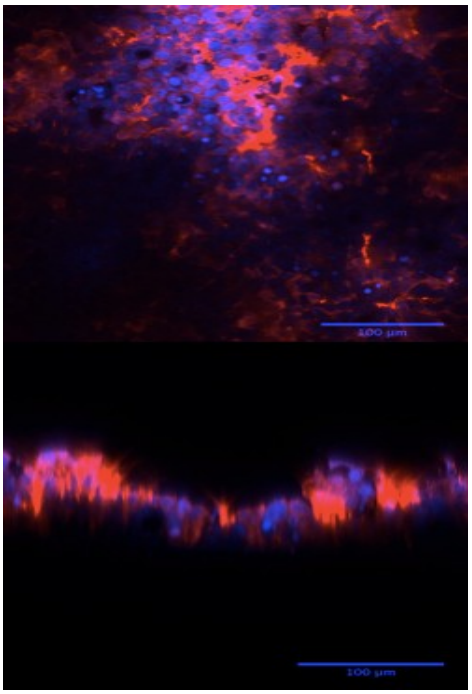

Figure 2.2.3. (GC) on CaCo-2 intestinal epithelium equivalent. . Polystyrene nanoparticles were coated with Glycol RhodamineB-Chitosan. In Z and in Y view it is clear the deep distribution of the polymer.

2.5.6 Conclusions

Based on LbL technique represents a very attractive tool for the realization of drug delivery systems (DDSs) with ideal features like simplicity, versatility, and nanoscale control. The aim of this part of research activity concerns the *in vitro* evaluation of completely biocompatible and biodegradable nanocarriers with diverse functionalities and different drugs.

Starting from natural materials like soybean oil and egg lecithin as surfactant they were realized nanoscaled oil-core carriers in which hydrophobic drugs or contrasting agents have been successful encapsulated.

The O/W nanoemulsions proposed by Vecchione *et al*. [106] possess relevant characteristics. Due to the use of a high pressure homogenizer the O/W emulsion obtained has a tunable size ranging from 80 to 200 nm (depending on the pressure applied and the surfactant used) with an excellent size distribution (PDI below 0.1). The so realized nanoemulsion has been used as liquid core for the realization of oil-core polyelectrolytes-shells nanocarriers. As for the liquid core, natural materials have been selected also for the realization of the shell, and, in particular, polysaccharides and polyaminoacids. [120-123]

Starting from these conditions this research part has focused on the modifications of the chitosan used as coating in order to add desired functionalities to the final nano-vectors and besed on epithelial cells properties. In fact, while in **Chapter 2** a nanoemulsion was loaded with curcumin and coated with a modified chitosan (with thiol

moieties) (GCNAC) is presented as an oral delivery nanocarrier tested on a healthy tissue and for a general evaluation of this particular benefical curcuma longa used as nutraceuticals. *In vitro* tests tried to clarify the routes of the nanosystem and, in particular, how it interacts and passes the intestinal barrier and the effect on the curcumin assimilation and anti-inflammatory activity.

Instead in **Chapter 3**, glycol chitosan (GC) was chosen as a polymer due to a deep penetration of the nanocapsules and the encapsulated drug was PXL according to its chemoterapic properties and it was tested on a 3D intestinal tumoral model.

2.7 References

[92] J.A. Uranga, V. López-Miranda, F. Lombó, R. Abalo, Food, nutrients and nutraceuticals affecting the course of inflammatory bowel disease, Pharmacological Reports, 68 (2016) 816-826.

[93] S. Kalepu, M. Manthina, V. Padavala, Oral lipid-based drug delivery systems–an overview, Acta Pharmaceutica Sinica B, 3 (2013) 361-372.

[94] C. Araujo, L. Leon, Biological activities of Curcuma longa L, Memorias do Instituto Oswaldo Cruz, 96 (2001) 723-728.

[95] B.B. Aggarwal, K.B. Harikumar, Potential therapeutic effects of curcumin, the anti-inflammatory agent, against neurodegenerative, cardiovascular, pulmonary, metabolic, autoimmune and neoplastic diseases, The international journal of biochemistry & cell biology, 41 (2009) 40-59.

[96] Y.-J. Wang, M.-H. Pan, A.-L. Cheng, L.-I. Lin, Y.-S. Ho, C.-Y. Hsieh, J.-K. Lin, Stability of curcumin in buffer solutions and characterization of its degradation products, Journal of pharmaceutical and biomedical analysis, 15 (1997) 1867-1876.

[97] P. Basnet, N. Skalko-Basnet, Curcumin: an anti-inflammatory molecule from a curry spice on the path to cancer treatment, Molecules, 16 (2011) 4567-4598.

[98] R. Vecchione, V. Quagliariello, D. Calabria, V. Calcagno, E. De Luca, R.V. Iaffaioli, P.A. Netti, Curcumin bioavailability from oil in water nano-emulsions: In vitro and in vivo study on the dimensional, compositional and interactional dependence, Journal of Controlled Release, 233 (2016) 88-100.

[99] S. Miret, L. Abrahamse, E.M. de Groene, Comparison of in vitro models for the prediction of compound absorption across the human intestinal mucosa, Journal of biomolecular screening, 9 (2004) 598-606.

[100] P. Artursson, K. Palm, K. Luthman, Caco-2 monolayers in experimental and theoretical predictions of drug transport, Advanced drug delivery reviews, 46 (2001) 27-43.

[101] J. Karlsson, P. Artursson, A method for the determination of cellular permeability coefficients and aqueous boundary layer thickness in monolayers of intestinal epithelial (Caco-2) cells grown in permeable filter chambers, International journal of pharmaceutics, 71 (1991) 55-64.

[102] I. Hubatsch, E.G. Ragnarsson, P. Artursson, Determination of drug permeability and prediction of drug absorption in Caco-2 monolayers, Nature protocols, 2 (2007) 2111-2119.

[103] F. Yokoyama, Y. Sakata, A. Ootani, T. Fujise, T. Kakimoto, S. Amemori, R. Shiraishi, T. Kuroki, S. Tsunada, R. Iwakiri, Differentiation of gastric surface mucous cells (GSM06) induced by air–liquid interface is regulated partly through mitogen‐activated protein kinase pathway, Journal of gastroenterology and hepatology, 22 (2007) 2310-2315.

[104] C. Nossol, A.-K. Diesing, N. Walk, H. Faber-Zuschratter, R. Hartig, A. Post, J. Kluess, H.-J. Rothkötter, S. Kahlert, Air–liquid interface cultures enhance the oxygen supply and trigger the structural and functional differentiation of intestinal porcine epithelial cells (IPEC), Histochemistry and cell biology, 136 (2011) 103-115.

[105] M. Natoli, B.D. Leoni, I. D'Agnano, F. Zucco, A. Felsani, Good Caco-2 cell culture practices, Toxicology in Vitro, 26 (2012) 1243-1246.

[106] R. Vecchione, U. Ciotola, A. Sagliano, P. Bianchini, A. Diaspro, P. Netti, Tunable stability of monodisperse secondary O/W nano-emulsions, Nanoscale, 6 (2014) 9300-9307.

[107] V. Calcagno, R. Vecchione, A. Sagliano, A. Carella, D. Guarnieri, V. Belli, L. Raiola, A. Roviello, P.A. Netti, Biostability enhancement of oil core — polysaccharide multilayer shell via photoinitiator free thiol-ene 'click' reaction, Colloids and Surfaces B: Biointerfaces, 142 (2016) 281-289.

[108] P. Artursson, T. Lindmark, S.S. Davis, L. Illum, Effect of chitosan on the permeability of monolayers of intestinal epithelial cells (Caco-2), Pharmaceutical research, 11 (1994) 1358-1361.

[109] L. Vijapur, S. Sreenivas, S. Patil, P. Vijapur, P. Patwari, Saraswathi, Thiolated chitosan: A novel mucoadhesive polymer: A review, International Research Journal of Pharamcy, 3 (2012).

[110] B. Wahlang, Y.B. Pawar, A.K. Bansal, Identification of permeability-related hurdles in oral delivery of curcumin using the Caco-2 cell model, European Journal of Pharmaceutics and Biopharmaceutics, 77 (2011) 275-282.

[111] E. Liang, K. Chessic, M. Yazdanian, Evaluation of an accelerated Caco□2 cell permeability model, Journal of pharmaceutical sciences, 89 (2000) 336-345.

[112] Y.-W. Jiang, H.-Y. Guo, Z. Chen, Z.-W. Yu, Z. Wang, F.-G. Wu, In Situ Visualization of Lipid Raft Domains by Fluorescent Glycol Chitosan Derivatives, Langmuir, 32 (2016) 6739-6745.

[113] J. Smith, E. Wood, M. Dornish, Effect of chitosan on epithelial cell tight junctions, Pharmaceutical research, 21 (2004) 43-49.

[114] P. Pinton, J.-P. Nougayrède, J.-C. Del Rio, C. Moreno, D.E. Marin, L. Ferrier, A.-P. Bracarense, M. Kolf-Clauw, I.P. Oswald, The food contaminant deoxynivalenol, decreases intestinal barrier permeability and reduces claudin expression, Toxicology and applied pharmacology, 237 (2009) 41-48.

[115] B.B. Aggarwal, L. Deb, S. Prasad, Curcumin differs from tetrahydrocurcumin for molecular targets, signaling pathways and cellular responses, Molecules, 20 (2014) 185-205.

[116] B.B. Aggarwal, W. Yuan, S. Li, S.C. Gupta, Curcumin‐free turmeric exhibits anti‐inflammatory and anticancer activities: Identification of novel components of turmeric, Molecular nutrition & food research, 57 (2013) 1529-1542.

[117] Y. ABE, S. Hashimoto, T. HORIE, Curcumin inhibition of inflammatory cytokine production by human peripheral blood monocytes and alveolar macrophages, Pharmacological Research, 39 (1999) 41-47.

[118] A. Beloqui, M.Á. Solinís, A.R. Gascón, A. del Pozo-Rodríguez, A. des Rieux, V. Préat, Mechanism of transport of saquinavir-loaded nanostructured lipid carriers across the intestinal barrier, Journal of Controlled Release, 166 (2013) 115-123.

[119] M. Somchit, C. Changtam, R. Kimseng, T. Utaipan, M. Lertcanawanichakul, A. Suksamrarn, W. Chunglok, Demethoxycurcumin from Curcuma longa rhizome suppresses iNOS induction in an in vitro inflamed human intestinal mucosa model, Asian Pac J Cancer Prev, 15 (2014) 1807-1810.

[120] D.K. Podolsky, V. Innate mechanisms of mucosal defense and repair: the best offense is a good defense, American Journal of Physiology-Gastrointestinal and Liver Physiology, 277 (1999) G495-G499.

[121] Vijapur L, Sreenivas S, Patil S, Vijapur P, Patwari P. 2012. Saraswathi, Thiolated chitosan: A novel mucoadhesive polymer: A review. International Research Journal of Pharamcy 3(4).

[122] F. Alexis, E. Pridgen, L. K. Molnar and O. C. Farokhzad, *Molecular pharmaceutics*, 2008, **5**, 505-515.

[123] V. P. Torchilin, in *Drug delivery*, Springer, 2010, pp. 3-53.

[124] Angela Langella[1,2,3+], Vincenzo Calcagno[1,+], Vincenza De Gregorio[1], Francesco Urciuolo[1], Giorgia Imparato[1,*], Raffaele Vecchione[1,*], Paolo A. Netti[1,2,3] "*In Vitro* Study of Intestinal Epithelial Interaction with Engineered Oil in Water Nanoemulsions Conveying Curcumin", Submitted on CSB August 2017.

Chapter 3

“3D colorectal cancer model for paclitaxel loaded engineered O/W nanoemulsion”

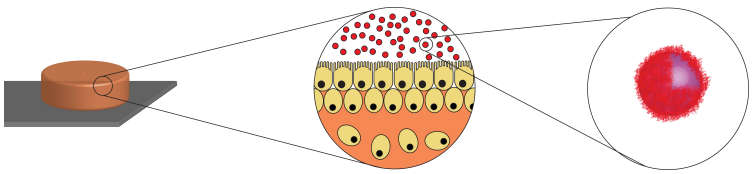

Abstract

Cancer is a complex pathology and current 2D in vitro-based cancer models do not accurately recreate the complex multi-cellular, 3D tumour microenvironment seen in vivo; as a consequence, a 3D cancer model is sorely needed not only for studying the complex disease processes ex vivo, but especially for performing reliable preclinical drug screening. Additionally, there is a growing interest in directing therapeutics towards the stroma, rather than the cancer cells, as stromal cells represent a more genetically stable target that is less likely to develop resistance. Since the clinical oncologist's arsenal of cancer therapeutics increasingly relies on biologically targeted compounds directed at signalling pathways related to the surrounding tumour microenvironment, an accurate *ex vivo* model that better replicates this microenvironmental complexity is required.

In this perspective, it is widely regnized that the majority of *in vitro* models cannot replicate the complexity of tumoral ECM leading the understanding of therapeutic strategy (i.e. nanocapsules) route very difficult. Here, to better mimic the *in vitro* tumor physiology that includes functional and morphological changes, a novel 3D intestinal cancer model is proposed. We present this model as an optimal platform for studying antitumoral mechanism of paclitaxel incapsulated in an O/W nanoemulsion coated with a functionalized polymer.

Introduction

3.1 Colorectal Cancer

In the last years, colorectal cancer has become a predominant cancer and now accounts for approximately 10% of cancer-related mortality in western countries. The ‘rise’ of colorectal cancer in developed countries can be attributed to the increasingly ageing population, unfavourable modern diet, habits and an increase in risk factors, such as smoking, low physical exercise and obesity. The change in incidence is not only apparent in the rates of sporadic disease but also in some familial cancer syndromes. [125]

Factors and risk conditions can be:

- **Age:** the incidence of CRCs increases with the age of the subject. It rarely affects people under the age of 50. CRC cases in young adults are associated with family predisposition conditions
- **Familiarity:** presence of first and second-degree relatives with familial adenomatic polyposis (FAP) or non-polypotic colorectal cancer (HPNCC) increases the risk of contracting CRC
- **Smoke:** smokers are more likely to die for CRC outcomes than non-smokers. An American Cancer Society study states that "smoker women have a greater chance (40%) to die for CRC than non-smoking women". Similarly, "smoking men are more likely to die (30%) for CRC than non-smokers.
- **Diet:** the high content of fat and protein in the diet increases the onset of CRC in relation to the carcinogenic potential of

cholesterol protein catabolites. Other studies confirm the importance of fiber and fruit consumption as a protection factor. In particular, vitamins and fruit antioxidants, such as vitamin C, are able to protect colonic cells from oxidative stress.

- **Ambiental Factors:** people who lives in industrialized areas have a greater risk of CRC development
- **Chronic inflammatory bowel processes:** such as chronic disease and ulcerative retortitis. About 1% of CRC patients have a history of ulcerative retalkitis. The risk of developing CRC is directly related to the severity of injury to the intestinal mucosa and to the extension of the inflammatory process. The risk of developing CRC in subjects with chron disease is lower than those with ulcerative retouchitis.
- **Hormones:** differences in the incidence and age of males and females can be attributed to the different hormonal pattern between the two sexes; In particular, the emphasis is placed on estrogen. The presence of conflicting data makes these studies still unreliable. Indeed, an increase in CRC was reported in women who underwent substitution therapy for estrogen (tamoxifen), as opposed to the hypothetical protective role of female hormones.
- **Presence of polyps in the colon:** isolated polyps may have areas of proven malignancy. Conversely, in localized colon cancer carcinoma there are adenomaous areas due to previous polypoid formation.

The site of onset of polyps is often the site of CRC's onset. Subjects with polyps are more likely to develop CRC than healthy subjects.

The more polyps are diagnosed in the subject, the greater the likelihood of developing CRCs (Figure 3.1).
Polypectomy reduces the onset of CRC. Prognosis in subjects with colorectal cancer depends heavily on the degree of local tissue invasion, the infiltration of nearby organs, and the presence of lymph node metastases and other organs. [126-129]

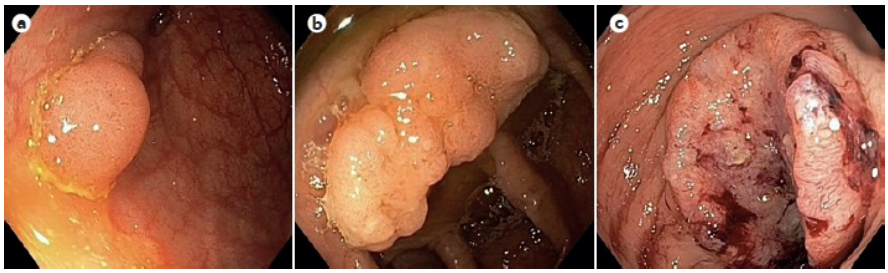

Figure 3.1) Colorectal neoplasia at different stages. A) A small sessile adenoma. **B)** An advanced, larger sessile adenoma. **C)** A large, dish-shaped, ulcerating sigmoid carcinoma. The tumour covers most of the circumference, but has not yet led to substantial obstruction of the lumen. Adapted from [125].

3.2 Advantages of 3D modeling *vs* 2D

The growth and maintenance of a human tissue depend on essential factors such as cell-cell interactions through growth factors, hormones and adhesion molecules. An ECM is essential in order to provide mechanical support capable of regulating cellular functions and synthesis of biological nutrients and effectors that can support tissue differentiation and maturation. 2D models, while being widely used, are limiting the study of tumorigenic and in providing affidable

results during *in vitro* tests. [130] Despite significant improvements in cancer field, researchers are still working to find new and effective therapies against cancer. Part of the issue is the lack of suitable preclinical models capable of recapitulate the complexity of cancer disease. The colorectal cancer is a pathology that affects neoplatic cells as well as the entire cell surroundings. Tumor microenvironment is a complex milieu comprising cancer and non-cancer cells embedded into the ECM. [131]

The interstitial matrix of the ECM consists of fibrillary collagens, proteoglycans and glycoproteins. [132] All these elements of the microenvironments are influenced by cancer cells and in turn influence tumor genesis and progression. [133] *In vitro* human small intestine models play a crucial part in preclinical drug development. Although conventional 2D systems possess many advantages, such as facile accessibility and high-throughput capability, they can also provide false results because of lacking physiological relevance. Significant progresses have recently been made in developing 3D human small intestine models, suggesting that more-reliable preclinical results could be obtained by reproducing *in vitro* 3D human small intestine model. This includes cells cultured as multicellular aggregates (spheroids) and cells embedded into natural (such as Matrigel, Fibrin or Collagen) or synthetic matrices (such as PLG, PLA, PEG) generally cultured in multiwell or into microfluidic devices. [134] Lot of them do not recapitulate the actual environment in which cancer cells are found *in vivo*. In fact, spheroids are characterized by low collagen [135] and natural or synthetic matrices. This system effectively does not replecate the physiological complexity of the microenvironment typically associated with

advanced carcinoma *in vivo*. Another recent culture system involves cell seeding on fibroblasts 3D matrices but these are commonly murine. [136-137]

In order to develop new target strategies, it is neecessary to consider the importance of the ECM. Jiajie Yu *et al*. [138] affirm that 3D human intestinal model has the potential to facilitate drug screening and drug development. Significant progress has recently been made in developing 3D human small intestine models, suggesting that more-reliable preclinical results could be obtained by recreating the 3D intestinal microenvironment *in vitro.* Thus, it has always been known that *in vivo* animal models too often fail to represent the pathology of human tumors, for this purpose the need to develop several *in vitro* models is high.

3.3 *In vitro* 3D tumoral intestinal model for drug delivery tests

The models generated through recent 3D culture systems can meet the basic requirements for recreating a human tissue and being used as preclinical tumor models for drug delivery or drug release. 3D cellular models can accurately reproduce the tumor micro-environment and mimic the regulatory mechanisms that cross between tumor and stroma. The 3D cell cultures exhibit peculiar molecular characteristics that are also significantly different from monolayer cultures and they are closer to the structural structure of the tissue *in vivo*. For this reason, when the object of the study is a tumoral tissue, this kind of tissue architecture shows that epithelial tumor cells undergo variations in shape and polarity, typically

associated with *in vivo* tumor progression. [139] Currently, the most popular 3D model is a multicellular tumor spheroids (MCTS), or organoids and tumoroid. The definition of these terms is very controversial in literature. In fact, they consist of tumor cells or a co-culture of tumor and thrombotic cells that acquire a spherical symmetry organized in three-dimensional order. Spheroids are generally produced by stabilized cell lines that aggregate in a homotypical manner and exhibit morpho-physiological characteristics that favor complex cell-cell and cell-matrix interactions. [140] These characteristics make them comparable to vascular tumor regions and / or micro-metastases *in vivo*. Tumor cells within the spheroid reproduce the same concentric arrangement and at the same time have a growth pattern similar to solid tumors in the non-vascular initial space. These features make multicellular tumor spheroids a system closer to the *in vivo* tumor structure and make them an excellent alternative to the study of different tumors. Due to their peculiarities they are a good model for testing antitumor drugs or to evaluate the gene expression of tumor cells during neoplastic development. Although the spheroid method is a promising approach, it has some disadvantages. In the first place, the spheroids form large aggregates that show a central necrotic core and this technique not is suitable for large scale and for a long-term studies.

Recently, Brancato *et al.* [141] demonstrated that spheroid and microtissue posses different “tissue mimicking capability”. They prove that 3D system promotes the assembly of ECM that better replicates the functional differences existing *in vivo* between normal and cancer-activated tissue in terms of cell growth, cell metabolim, metabolic and mechanical microenvironment and ECM composition.

For this reason, the 3D model would increse the predictive potential of both tumor-on-chip system, and drug screening platform (figure 3.4). Another good revolution for intestinal 3D tissue realization was made by Sato *et al*. [142] successfully cultured murine epithelial organoid from single Lgr5+ intestinal stem cell (ISC) *in vitro*. Subsequently, human pluripotent stem cell (hPSC)-derived intestinal organoid (HIO) [137] and organoids derived from human normal and diseased biopsy samples were developed. [143] These 3D, self-organized, physiologically relevant cellular structures can be grown long-term and remain genomically stable.

These systems have already proven to be useful in studies of GI tract development, homeostasis, human-microbiome symbiosis, and pathogenesis and for drug delivery screening.

Here, we propose the realization of human 3D colorectal cancer tissue as platform for study the effects of enginereed paclitaxel-loaded nancapsules. By exploiting the affinity with the cellular model, nanoapsules can releases in a specific and deep way the drug in this case paclitaxel, overcoming a whole set of limitations of conventional anticancer therapy.

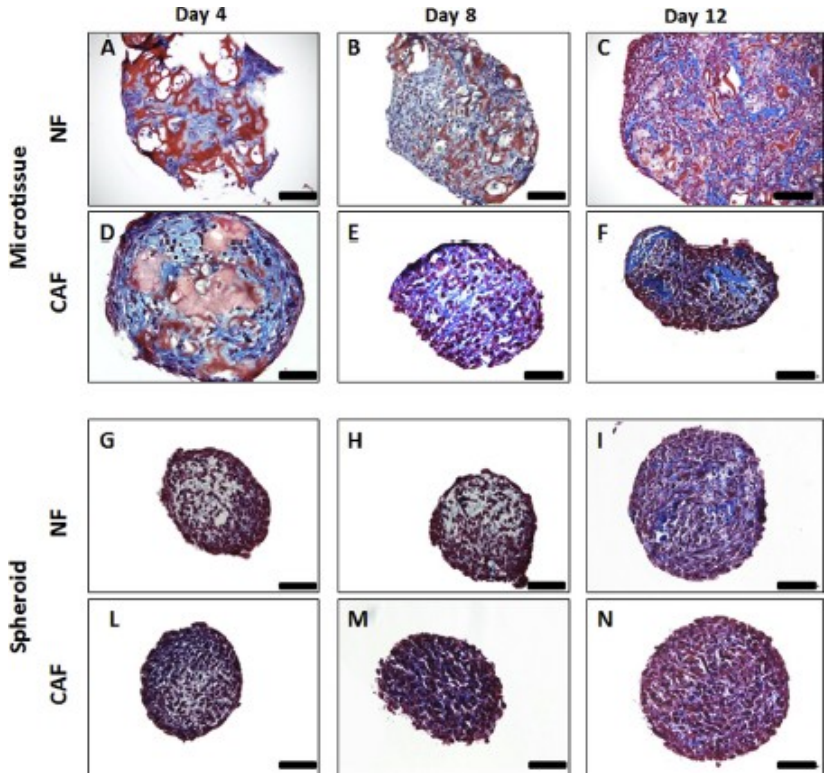

Figure 3.4: Masson Trichrome images of NF-lTP (A–C), CAF-lTP (D–F), NF-sph (G–I) and CAF-sph (L–N) at Day 4, Day 8 and Day 12. Collagen in blue, cell nuclei in purple. Initial gelatin microsphere when present appear stained in red/brown. Scale bar is (A–C) 100 lm, (D–N) 50 lm. Adapted from [141].

3.4 Our approach: tissue modules realization

Our approach is proposed as a bottom up method to build up 3D tissue constructs *in vitro* by using microtissues (μtP) as functional building units. μtP modules have been obtained by means of dynamic cell seeding of fibroblasts on porous gelatine microcarriers using a spinner flask bioreactor as depicted in step 1 of (figure 3.2A). Several studies demonstrated that this particle cultivation technique is more effective than cell culture on flat substrates such as culture dishes. [143] Under optimal culture conditions, cells were able to adhere, proliferate, and, in particular, synthesize ECM components to form a thin layer of de novo-produced tissue around the microbeads. This micrometric tissue wrapped around and within the porosity of the scaffold constitutes micrometric tissue precursors (μtPs) for further large-tissue construction. [144] The process for μtP formation consisted of a dynamic cell seeding performed in a spinner flask bioreactor, which was loaded with cells and porous gelatine microbeads in the ratio of 11-13 cells per microbead and operated at 20 rpm for 10 days. The disappearance of free cells from the inoculated spinner cultures was considered to indicate the attachment of cells to the microcarriers.

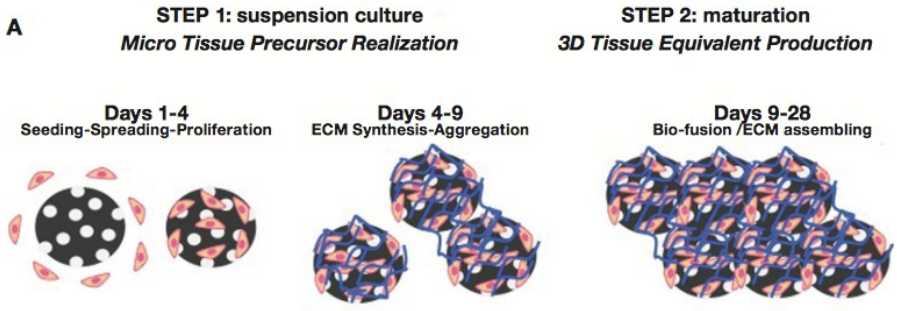

Figure 3.2. Description of 2 STEP process used to generate 3D tissues *in vitro*. cell seeding and micro-scaffold colonization at an early time; ECM synthesis and formation of small aggregates named µTP; **(A)** fusion and assembly of µTP to produce large 3D tissues.

3.4.1 µTPs assembly and maturation chamber

To obtain a single and compact macro tissue of the desired shape and thickness, the µTP suspension was withdrawn from the spinner flask and transferred and cultured in an assembling chamber (Figure 3.3B). The assembling chamber has a sandwich-like structure (Figure 3.3Ba), in the middle of which there is a silicon mould with four empty spaces (1 mm in thickness, 10 mm in diameter, Figure 3.3Bb), where the µTPs assembly takes place. The silicon mould is delimited on both the top and bottom sides by two stainless steel rigid grids (Figure 3.3c) characterized by a porous mesh (18 lm) that is able to retain the µTPs. Two polytetrafluoroethylene (PTFE) rings (Figure 3.3Bd) are placed on the grids on both sides of the system and are fastened to each other by means of stainless steel screws, which close the system and ensure that the µTPs are retained. The system is autoclavable in each part. The µTP suspension was transferred from

the spinner flask to a 50 ml Falcon centrifuge tube and, after settling, transferred by pipetting into the empty spaces of the silicon mould of the assembling chamber (Figure 3.3B) to allow the assembly. Furthermore, the assembling chamber was placed in a spinner flask and filled with culture medium. The spinner was operated at 50 rpm and the medium was exchanged every 2 days. After 4-5 week of culture the assembling chamber was opened and the biohybrids were collected for different analysis.

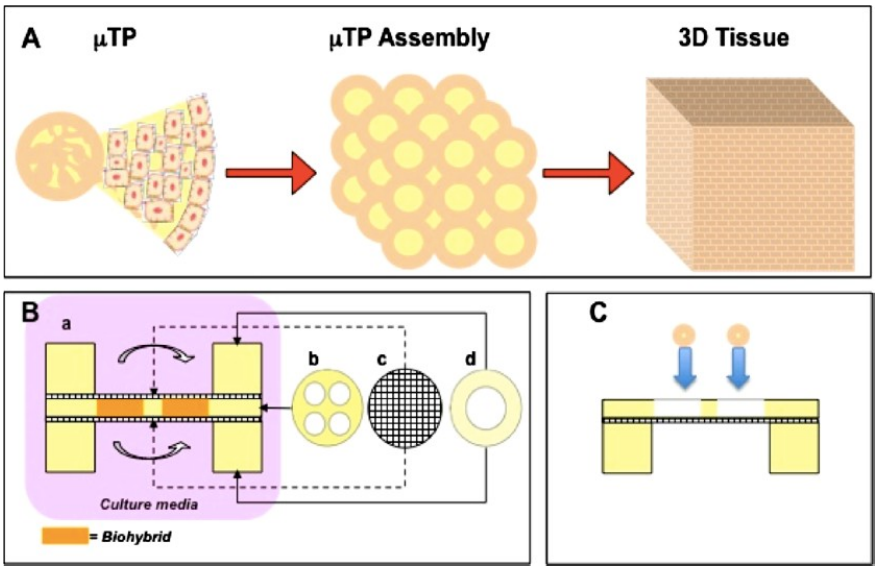

Figure 3.3: A bottom-up approach was proposed to build up 3-D tissue constructs *in vitro* by using µTPs as functional building units. The process philosophy is schematized. Adapted from [144].

3.4.2 Realization of 3D human equivalent model

Seeding human epithelial cells like keratynocytes, Caco-2, Hct116, and some other types of epithelial cells on this kind of matrix allowed obtaining a functional tissue equivalent model in which it is possible to generate structures *in vitro* resembling the *in vivo* features. [145]

3.4.3 O/W Nanoemulsion loaded with Paclitaxel for drug delivery test on 3D intestinal diseased model

PXL is a common chemotherapeutic that has been used clinically for many years to treat ovarian, breast, lung, and pancreatic cancer. It is also an approved chemotherapeutic in the UK for ovarian, breast, lung, bladder, prostate, and other types of solid tumors as well as melanoma and Kaposi's sarcoma. [146] Recent studies have shown the effects of PXL also in coloncancer. The mechanism of action of PXL involves interference with the process of normal breakdown of microtubules during cell division, causing apoptosis in the treated cells. [147-149] The solubility of PXL hinders its application in the clinic. In addition, PXL can cause some side effects such as hypersensitivity reactions, myelosuppression, and peripheral neuropathy. [150] This makes the nanodrug delivery system a useful tool to assist with PXL solubility and delivery. Lipid nanocapsule-loaded PXL was also shown to be more effective for oral administration with enhanced bioavailability. [151] Nanoemulsion is another attractive way to deliver the hydrophobic drugs such as PXL,

and some studies have demonstrated that nanoemulsion loaded PXL can overcome drug resistance [152-153] increase cellular uptake, [154-155] and enhance cytotoxicity and apoptosis in different cancer cells. [156] In colorectal carcinoma, several previous studies have shown that PXL could inhibits tumor cell growth by regulating glutaminolysis in colorectal carcinoma cells. [157] Mounting evidence indicates that altered glutamine metabolism in cancer cells has critical roles in supporting macromolecule biosynthesis, regulating signaling pathways, and maintaining redox homeostasis, all of which contribute to cancer cell proliferation and survival. Thus, intervention in these metabolic processes could provide novel approaches to improve anti-cancer treatment. [158] Our nanocapsules are able to reduce cells invasion and metastatis in colorectal cancer, due to their capability to increase PXL solubility and enanche the crossing because of functionalized polymer modification (GC).

3.2 Materials and methods

1-hydroxybenzotriazole hydrate (HOBt), N-acetyl-L-cysteine (NAC), Rhodamine B isothiocyanate (RBITC), paraformaldehyde and curcumin (from Curcuma Longa Turmeric), powder, m.w. = 368.38 g/mol) were purchased from Sigma-Aldrich. (GC) was purchased from Wako Chemicals. 1-(3-dimethylaminopropyl)-3-ethyl-carbodiimide hydrochloride (EDC) was purchased from Iris Biotech. CaCo-2 cells were obtained from American Type Cell Culture (ATCC, Usa). Dulbecco's Modified Eagle's Medium (DMEM, Gibco, Life Technologies), supplemented with 10% fetal bovine

serum (FBS, Sigma Aldrich), 1% penicillin/streptomycin and 1% L-glutamine (Lonza, Milan) and 2% nonessential amino-acids NEEA (Euroclone, Milan). Hank's balanced salt solution (HBSS) was purchased from Gibco, Life Technologies. Transwell permeable supports (24-well plates with polyester membrane 0.4 μm) were purchased from Corning® Costar. FITC-Dextran was purchased from Molecular probes, Life Technologies. Trypsin was purchased from (Lonza). High pure RNA tissue kit was purchased from Roche. Transcriptor First Strand cDNA synthesis kit was purchased from Roche. SYBR® Green Master mix was purchased from Aurogene (2x SensiFaST SYBR). Primer of GLS, SLC1A5, SLC7A11 was purchased from Metabion.

3.2.1 Cells culture

Human dermal fibroblasts (HDFs) were extracted from healthy foreskin or breast biopsies and cultured in enriched MEM: MEM (Microtech L0440-500) with 20% of FBS (Sigma Aldrich), 2% of Non-Essential Aminoacids (EuroClone ECB3054D), 1% of L-Glutamine (Lonza 17-605E) and 1% of penicillin/streptomycin (Microtech L0022-100), until passage 4/7.
InMyoFibroblasts were seeded into a flask and cultured with the apposite supplemented medium SMBM/SMGM by Lonza.

3.2.2 HDFs and inMyoFibroblastas source

Cells were extracted from human tissue biopsies surplus obtained by "Azienda Ospedaliera di Rilievo Nazionale e di Alta Specializzazione

(AORN) A. Cardarelli/Santobono/Pausillipon at Urology and Biotechnology Centre - AORN" according to the project "Realization of human skin equivalent *in vitro*" after approval of ethical committee. Even if, InMyFibroblast were pruchuased by Lonza.

3.2.3 Micro-scaffold production

Gelatin porous microbeads (GPMs) were prepared according to a modified double emulsion protocol (O/W/O). GPMs were stabilized by crosslink reaction with glyceraldehyde (GAL) (SIGMA-G5001), in order to make them stable in aqueous environment at 37 °C, as previously described. GAL at 4% w/w of the microbeads was used to perform all the experiments.

3.2.4 Micro-tissues (µTPs) production

About 13 HDFs p5/8 were seeded for each bead. Cells were cultured into spinner flask bioreactor (Integra) in continuous agitation (30 rpm) after 6 hours of intermitting stirring regime in order to promote cell seeding (30 min at 0 rpm, 5 min at 30 rpm). The culture medium was enriched MEM plus Ascorbic Acid (2-O-α-D-105 Glucopyranosiyl-L-Ascorbic-Acid TCI; Cf: 0.5mM). µTPs were cultured for 9 days before the phase of assembly in order to guarantee the initial collagen synthesis.

3.2.5 Intestinal equivalent model production

During the microtissue assembly the μTPs suspension was transferred from the spinner flask to a 50 ml Falcon centrifuge tube and, after settling, transferred by pipetting into the maturation chamber to allow their molding in disc-shaped construct (1 mm in thickness, 8 mm in diameter). During the filling procedure, the maturation chamber was accommodated on a device connected with a vacuum pump to make the process faster and to assure that any bubble was in the maturation space. The assembling chamber was a sandwich-like structure with in the middle a silicon mold with empty spaces (disc shape: 1 mm in thickness, 8 mm in diameter; wire shape: 1 mm in thickness, 5cm length) for the μTPs housing. The silicon mold was delimited on both the top and bottom sides by two stainless steel rigid grids characterized by a porous mesh (18 μm) that was able to retain the μTPs and to guarantee the passage of nutrients and waste products. Two polytetrafluoroethylene (PTFE) rings were placed on the grids on both sides of the system and were fastened to each other by means of stainless steel screws, which close the system. The assembling chamber was placed on the bottom of a spinner flask (Bellco biotechnology code 1967- 00050) and completely surrounded by culture medium. The spinner was operated at 30 rpm. The culture medium was enriched SMDM and EMEM plus ascorbic acid. After 4-5 weeks of culture the assembling chamber was opened and biohybrids were collected.

3.2.6 Epithelial cell seeded on biohybrids

For the production of the 3D healty model, Human colonic epithelial cell line, CaCo-2 cells, were obtained from American Type Cell Culture (ATCC, USA) and were grown in Dulbecco's Modified Eagle's Medium (DMEM, Gibco) supplemented with fetal bovine serum (FBS, Sigma Aldrich), 2 mM/l L-glutamine (Gibco), 100 IU/ml streptomycin/penicillin (Gibco) at 37°C with 5 % CO_2. The cells were seeded at $1x10^5$ on 8 mm biohybrids and grown into a Transwell insert were biohybrids were tmoved on polycarbonate membrane for three weeks. During the first week cells grows till to completely cover all the biohybrid surface, thus leading to a submerged layer; during the second and third week the upper medium is removed and cells are capable to polarize, thus leading to an ALI. Medium was replaced every 2 days. While for the realization of a tumor 3D model the HCT116 were seeded at the same concentration and the same time were respected. The difference is the medium that was RPMI purchuased by Lonza and supplemented with fetal bovine serum (FBS, Sigma Aldrich), 2 mM L-glutamine (Gibco) 100 IU/ml streptomycin/penicillin (Gibco) at 37°C with 5 % CO_2.

3.2.7 Immunofluorescence on the 3D sample

Sample were fixed in 4% paraformaldehyde (P61148-500g Sigma Aldrich) for 30' at RT and washed in PBS. They were permeabilized using 0,1% Triton (Triton® X-100 T9284-100ML Sigma) in PBS for

5’ at RT, washed in PBS and blocked in 1%BSA (A9418-100G Sigma) for 1h at RT. Samples were stained with Rhodamine Ulex Europaeus Agglutinin I (UEAI Vector Laboratories RL-1062) at a final concentration of 20µg/ml in blocking solution, in order to mark the *endothelium*, overnight (ON) at 4°C in the dark. The morning after, samples were washed with PBS1X. The nuclei of all the cells were stained with Sytox Green (Invitrogen S7020) for 20’ at RT. Samples were fixed in PFA 4% and after washed for three times in PBS. After the samples were moved into a fluorodish 23mm and incubated for 1h with different concentrations of TBE and PBS 20% 40% 60% 80% and the last incubation with TBE 100% overnight at RT. Samples were investigated into the same fluorodish by Confocal Leica TCS SP5 II.

3.2.8 Histology on paraffin sections

Samples were fixed in Formalin 10% (HT501320 Sigma) for 1h at Room Temperature (RT) and washed in PBS (P4417-100TAB Sigma). They were dehydrated in Ethanol from 75% to 100% and treated with xylene (A9982 ROMIL) before the inclusion in paraffin. Tissue slices thick 7µm were cut using a microtome (Thermo Scientific HM 355S) and then deparaffinized using xylene. Sections were hydrated in ethanol from 100% to 75%, washed in water and stained using Hematoxylin/Eosin (Bio Optica W01030708). The sections were mounted with Histomount Mounting Solution (Bio Mount HM 05-BMHM500 Bio-Optica) on coverslips and the morphological features of µTPs were observed with a light microscope (Olympus, BX53).

3.2.9 Second harmonic generation signal

For SHG imaging samples were investigated by confocal microscopy (TCS SP5 II Leica) combined with a MPM where the NIR femtosecond laser beam was derived from a tunable compact mode-locked titanium: sapphire laser (Chamaleon Compact OPO-Vis, Coherent). Two-photon excited fluorescence was used to induce second harmonic generation (SHG) and obtain high-resolution images of unstained collagen structures. The samples were observed by using λ_{ex} = 840 nm (two photons) and λ_{em}=415-425 nm. The SHG images were acquired with a resolution of 12 bit, 512x512 pixel by using a 25X water immersion objective (HCX IRAPO L 25.0X0.95 Water, n.a. 0.95).

3.2.10 Molecular analysis

Biohybrid with HCT116 were weighed, cut and treated with 2,5mg/ml collagenase A (ROCHE) for 30 minutes. Samples in lysis buffer were placed into 2ml Eppendorf with a stainless-steel ball for mechanical digestion on a vortex. RNA extraction was performed by means of the high pure RNA tissue kit (ROCHE 12033674001) according to manufacturer's protocol. Lysates were centrifuged into high pure filter tube. The flow through was discarded and samples were incubated in presence of DNase and DNase incubation buffer for 15 minutes at RT. Washing buffer 1 with ethanol was added and samples were centrifuged for 10 seconds at 10.000 rpm and flow

through was discarded, so for washing buffer 2. After a second wash in buffer 2, samples were centrifuged for 2 seconds at 13.000rpm. Finally, RNA was eluted in 50µl of elution Buffer after centrifugation for 1 minute at 10.000rpm. RNA was quantified by means of spectrophotometer (Eppendorf Bio Photometer). 100ng of RNA were retro-transcribed using iScript™ reverse transcription supermix (Biorad 1708840). 4µl of super-mix and water were added to samples up to a final volume of 20µl. The complete reaction mix was incubated in a thermal cycler using the following protocol: 5 minutes at 25°C, 30 minutes at 42°C and 5 minutes at 85°C.

Real Time PCR was performed using BIORAD CFX96 Real-time system C100 Touch Thermal cycler. 2,5µl of cDNA were mixed with iQ™ SYBR® Green Super-mix (Biorad 170-8880), 0.6µl of forward and 0.6 µl reverse primers (from stock solutions 100µM) and water to a final volume of 10µl. All quantifications were normalized with the GAPDH mRNA level, then the fold induction was calculated by the ΔΔCt method.

Gene Name	Primer Sequence (5′to 3′)
GLS	F: 5′-GAGTACTGAGCCCTGAAGCAGTTCG-3′
	R: 5′GGAGACCAGCACATCATACCCA-3′
SLC7A11	F: 5′-AGAGGGTCACCTTCCAGAAAT-3′
	R: 5′-AGATAAATCAGCCCAGCAACT-3′
SLC1A5	F: 5′-GAGAAATATCTTCCCTTCCAACCTGG-3′
	R: 5′-CCAAAGACGATGGCAAACACTACC-3′

Table 3.1: **Primer sequences of GLS, SLC7A11 and SLC1A5 genes.**

3.2.11 Statistics

Experiments were performed in triplicate. Data are expressed as mean ± SD. Differences between groups were determined using the statistic test ANOVA Tukey HSD test. Significance between groups was established for p value<0.01 or p value<0,05.

3.3 Results and discussions

3.3.1 3D human colorectal cancer intestinal epithelial model

Nanotechnology-based systems such as nanocapsules, play an important role by enanching the efficacy for cancer therapy. The realization of 3D human colorectal cancer is really important for a good study of drug delivery and drug release. This kind of *in vitro* model are able to improve, more in detail, the influence of (ECM) in a molecular pathways invoved in cancer. The realization of disease 3D human intestinal model is finalized as an innovative platform for *in vitro* drug release, by exploiting the affinity with the cellular model, in a specific and deep way the drug, paclitaxel, overcoming a whole set of limitations of conventional anticancer therapy.

3.3.2 HD-µTP assembly assessment

The spinner flasks were loaded with 3,5 x10^6 cells and 54 mg of microbeads, corresponding to 15 cells per bead with an initial cellular density of 70,000 cells/ml and in a minimal volume of 50 ml. The first 8 h of the seeding phase were characterized in static mode, after 8 h the spinner flask goes overnight in an intermittent stirring to improve the cell-to-bead distribution and to obtain a lower proportion of unoccupied beads. [159] The disappearance of free cells from the

inoculated spinner cultures was considered to indicate the attachment of cells to the microcarriers. Only in this condition the spinner flask can go in a dynamic mode at 30 rpm for 10 days. Before proceeding with the loading of HD-μTP in the blank spaces of maturation chamber it was necessary to evaluate the aggregation of HD-μTP and deposition of an initial collagen matrix around and inside microcarriers. At 10 days of dynamic culture in spinner flask, HD-μTP appeared as 3D small compact aggregates composed of cells, evenly distributed around and inside the microbeads (Figure 3.4a). Masson Trichrome staining revealed the histological composition of HD-μTP, which aggregates of porous microbeads were surrounded by collagen (blue) and cells (violet) that proliferated exploiting the maximal available surface given by the interconnected porosity of GMPs (Figure 3.4b). Collagen deposition was confirmed by SHG signal (grey) (Figure 3.4c).

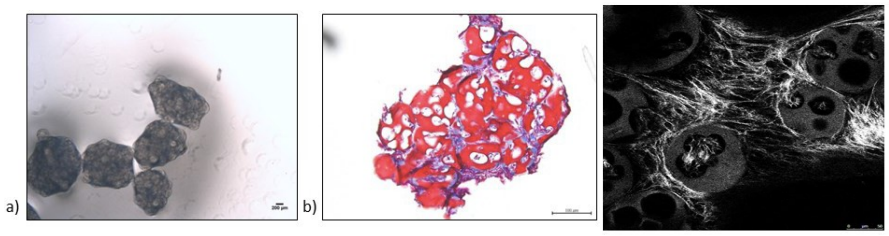

Figure 3.4. **HD-µTP analysis**. a) HD-µTP at optical microscope (Mag 4X); b) Masson Trichrome staining which showed cells around and inside microbeads (violet) and the ECM assembled (blue) surrounding 3D cell aggregates; c) SHG signal: collagen fibers were assembled around cells and held together microscaffolds and cells in a 3D µTP construct. Bars in a, is 100 µm; bar in b) Mag. 20X c) is 50 µm.

3.3.2 3D human intestinal stroma characterization

After HD-µTP assembly in the maturation chamber (Figure 3.5a and 3.5b), at the end of about 4 weeks of culture in the bioreactor (Figure 3.5c), we obtained a homogeneous and compact 3D human intestinal stroma equivalent model that preserved the shape and size after the removal from the chamber.

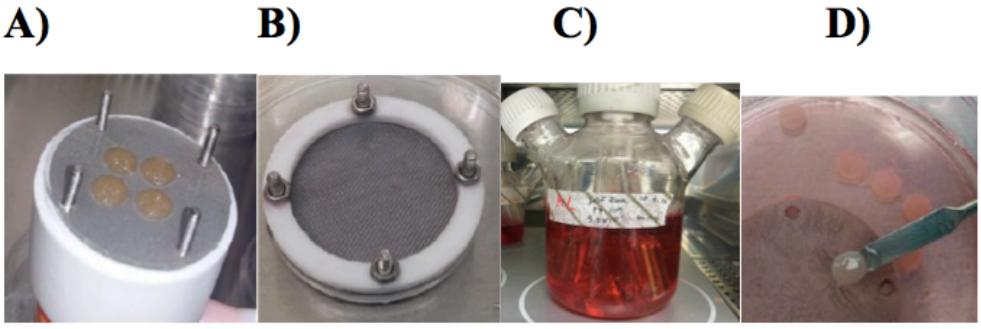

Figure 3.5 : **Intestinal stroma construction step by step**
(A) HD-µTP of 10 day of culture loaded in the maturation chamber; **(B)** maturation chamber sealed with grids, PTFE rings, screws and bolts; (**C)** bioreactor loaded maturation chamber sealed; (**D)** 3D intestinal equivalents obtained after 4 weeks of maturation in bioreactor.

3.3.3 3D human intestinal equivalent characterization

In order to develop a 3D full thickness human intestinal diseased model, human stroma equivalent tissues were extracted from chambers and prepared for HCT116 or CaCo-2 cells seeding. (Figure 5d) 3D full proliferation and differentiation of intestinal epithelial cells were cultured in transwell inserts in a traditional condition. During the submerged phase, 3D-intestinal equivalent were fully covered by medium, in order to allow cellular proliferation. After 7 days, samples were places in (ALI) favouring the cell polarization. The ALI time is around 10 days. After this period 3D samples are ready to some drug tests. (Figure 3.6)

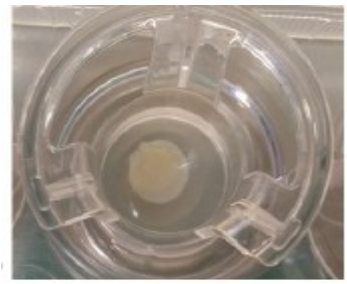

Figure 3.6: 3D human intestinal equivalent in a transwell insert after intestinal hct116 colorectal cancer cells seeding.

3.3.4 Healthy *vs.* tumoral 3D human intestinal model

Histology analysis allowed us to evaluate the distribution on the equivalent human stroma of the two types of cells.

CaCo-2 intestinal that mimic a healthy phenotype and which are on the surface of the equivalent human stroma are placing in an ordered and polarized epithelial cell layer. (Figure 3.7A) In the second image instead, the HCT116 cells, invasive cells of colorectal carcinoma are only partially on the epithelial surface, a lot of cells tend to migrate and invaded the extracellular matrix.(Figure 3.7BD) This type of analysis was also performed in the confocal microscope. Here, it is clear how cells are distributed by invading the stroma.(Figure 3.7C) These results confirmed what happens under *in vivo* condition, that is a principal charachteristic of colorectal carcinoma.

A) **B)**

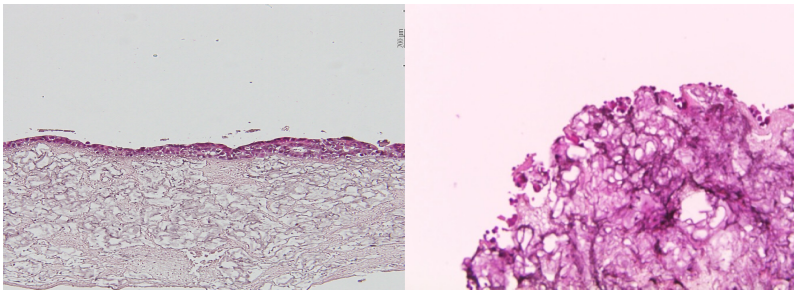

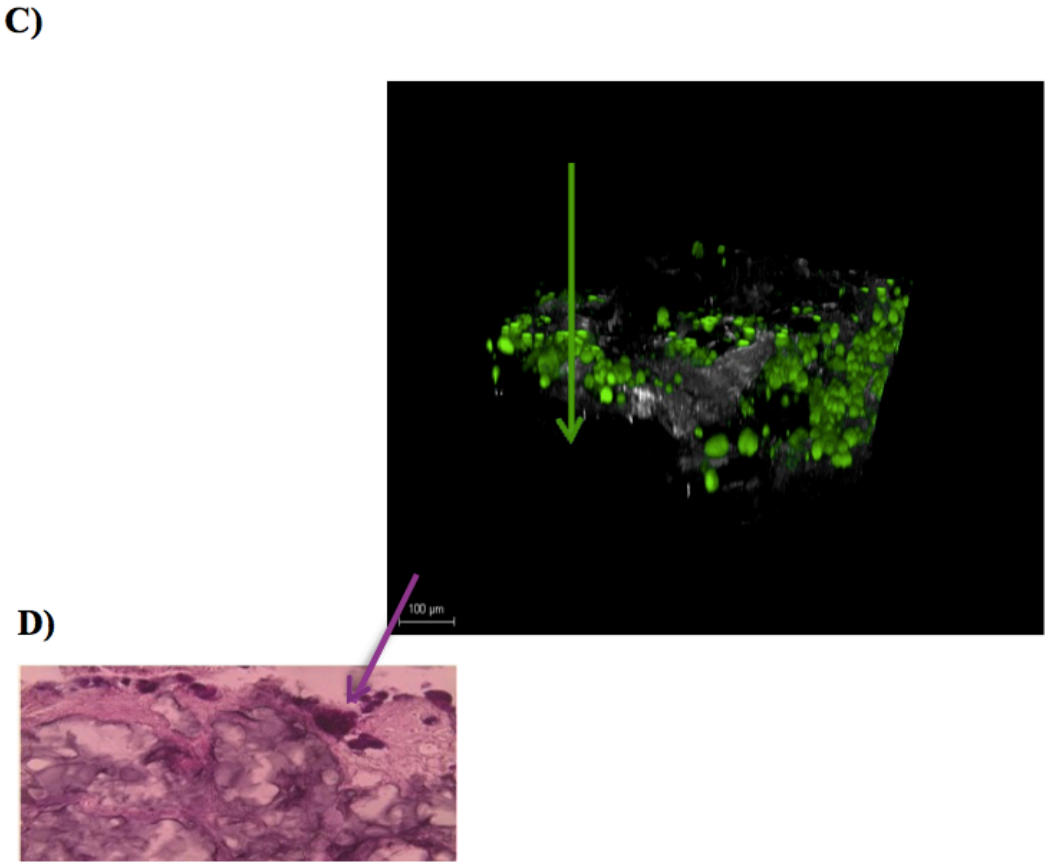

Figure 3.7: **3D tumoral intestinal model analysis: (A)** scale bar 200 µm and **(B)** Mag 20x respectively histologic and confocal images, it is clear that HCT116 colorectal carcinoma cells are able to reach the (ECM) and migrate for tumor invasion as *in vivo* conditions **(C)** scale bar 100 µm **(D)** Mag 40x.

3.3.5 *In vitro* 3D intestinal diseased model as platform to test paclitaxel loaded nanocapsules

In this study the aim was a deep penetration of the nanocapsules in the tissue, we used O/W nanoemulsion coated with glycol chitosan instead of modified glycol chitosan to avoid strong interaction between nanocapsules and mucus layer. This is in agreement with the observations previously described in chapter 2 (Supplementary results). These nanocapsules were loaded with paclitaxel and tested on the 3D intestinal disease model. After complete distribution of HCT116 seeded on 3D intestinal equivalent stroma, the test starts. The O/W nanoemulsion was loaded with 5µM paclitaxel with an encapsulation efficacy (> 95%) and coated with a specific designed polymer able to promote the permeability and solubility of the nanoemulsion through extracellular matrix in order to reach the HCT116 cells that after seeding invaded the human stroma quivalent. When the 3D intestinal diseased model reaches the optimum conditions, approximately after ten days, the test may begin. The paclitaxel loaded nanocapsules were suspended 1:1 in a poor colture medium: HBSS and put in contact with 3D intestinal diseased model housed in a transwell insert were a PDMS mold was used like sealed chamber, in order to confine the suspension of nanocapsules completely on the surface. (Figure 3.8) In this way it is avoided that it falls into the basolateral compartment. After 3h in the incubator at 37°C and 5% of CO_2 sample were rinsed 3 times with PBS and processed for different analysis.

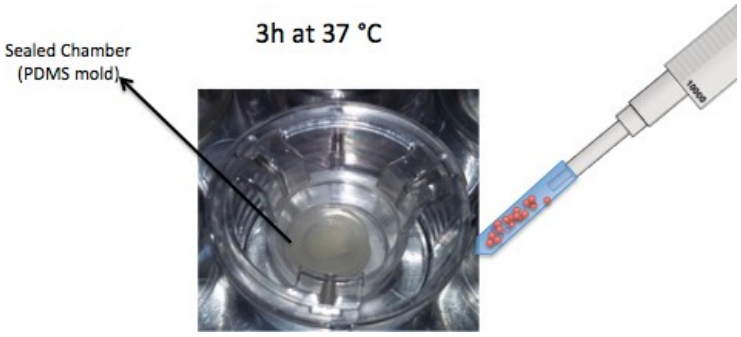

Figure 3.8: 3D intestinal tumoral model before the test. The sample was housed in a transwell insert with PDMS sealed chamber in order to confine the drop of paclitaxel loaded nanocapsules

3.3.6 Confocal imaging characterization of paclitaxel loaded nanocapsules and molecular effects: evaluation of the expression of glutaminolysis-related genes

Furthermore, confocal imaging was used to qualitatively visualize the transport and localization of paclitaxel loaded nanocapsules. (In Figure 3.9AB) we showed a 3D sections of 3D intestinal diseased model acquired with confocal microscope and elaborated with a software (Las-af X). GC coating was covalently labelled with Rhodamine B. This labelling, together with the specific staining of the biological sample, allowed to discriminate among paclitaxel loaded nanocapsules (red channel), cell nuclei (green channel) and collagen (grey channel). Confocal analysis highlighted the presence,

the localization and the transport of the proposed paclitaxel loaded nanocapsules. We demonstrated that, after 3 h, paclitaxel loaded nanocasules was distributed in the huma stroma equivalent, thanks to the presence of glycol groups that improve the capability of chitosan to permeate the tissue (Figure 3.9B). Hence, it can be noticed that they can cross the epithelium and rise the cells that have been invated the stroma. In order to confirm the paclitaxel loaded nanocapsules release paclitaxel, we also evaluated their anti-tumoral effect. Precisly we have evaluated the ability of paclitaxel to inhibits tumor cell growth by regulating glutaminolysis in colorectal carcinoma cells. To maintain a robust increase in nutrient uptake, in addition to increasing glycolysis, tumor cells commonly activate glutaminolysis. *GLS*, *SLC7A11* and *SLC1A5* genes play an important role in glutamate transport and metabolism. [158] After incubation, we evaluated the expression of glutaminolysis-related genes *GLS, SLC7A11* and *SLC1A5* that were significantly decreased in the colorectal carcinoma cells treated *versus* control that was treated with an empty O/W nanoemulsion (Figure 3.10).

Our results show that when the nanocapsules across the epithelia and go through the ECM they are capable of releasing PTX, which in turn, significantly decreases the expression level of glutaminolysis-related genes.

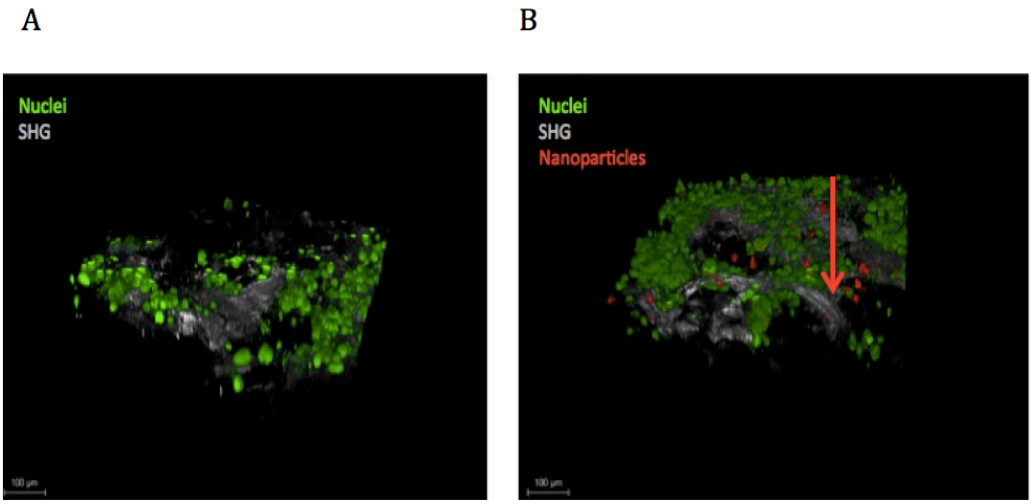

Figure 3.9: Confocal analysis of 3D intestinal tumoral model.
3D view of the samples: **A)** on the left ctrl and **B)** on the right 3h treated samples with Paclitaxel loaded nanocapsules.
In the treated samples nanoparticles across the 3D intestinal diseased model reaching also the cells that invaded the stroma.
Scale bar 100µm

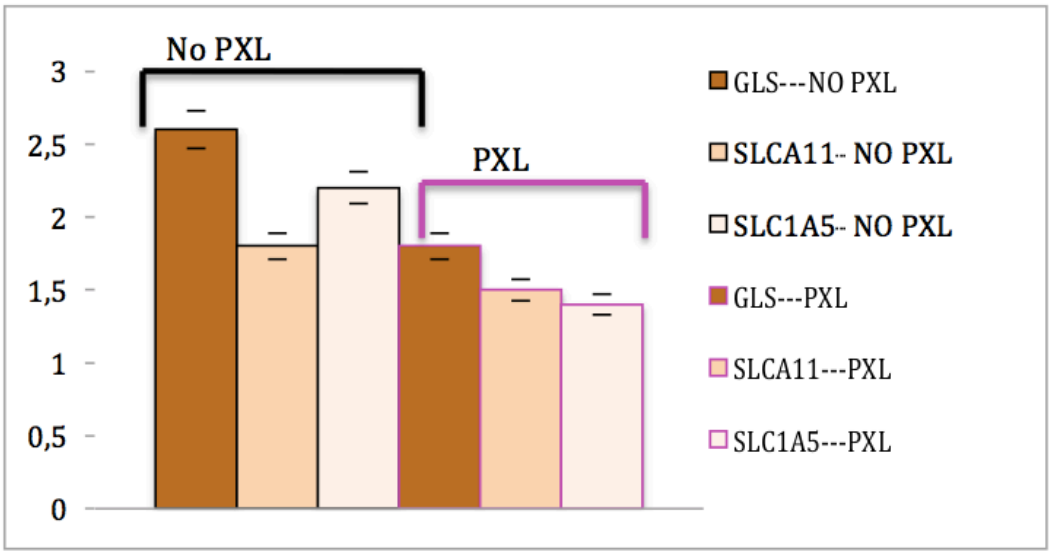

Figure 3.10: mRNA expression of glutaminolysis-related genes. Gene expression levels detected by quantitative real-time PCR assay after 3h treatment. The mRNA expression of GLS, SLC7A11 and SLC1A5. Data represent the means ± SD.

3.4 Conclusions and future perspectives

In conclusion, we developed a 3D complex tumoral intestinal *in vitro* model that due to the well-organized stromal micro-environment, represents a good platform for drug delivery systems. Therefore, it might be a promising tool for more predictive preclinical testings with pharmaceutical substances, probiotic active organisms, or chemoterapic agents based on tissue features.

The biological complexity of 3D tissue entails high requirements regarding applicable culture technique. In this context, 3D *in vitro* models can more realistically reproduce an organ target due to their complexity. According to the "3Rs" guiding principles for more ethical researches, 3D *in vitro* models can overcome the limitations of animal models, thus reducing the need for *in vivo* testing. Therefore, these models can offer a valid possibility for closing the gap between animal testing and drug administration to human subjects in clinical trials. Indeed, the better is the design of 3D models, the more significant is the reduction of the number of animals used for drug delivery systems studies *in vivo*.

In fact, in this thesis it was shown how is possible to move from 2D to 3D platforms for drug testing. The fact is that we are effectively able of creating both healthy and pathological cell assemblies.

In the light of this, the tissue engineering field is moving forward to its ultimate goal where organotypic systems can fully replace animal-based *in vivo* experimenting.

3.5 References

[125] Ernst J. Kuipers, William M. Grady, David Lieberman, Thomas Seufferlein, Joseph J. Sung, Petra G. Boelens, Cornelis J. H. van de Velde & Toshiaki Watanabe

[126] Harrison. Principi di medicina interna. New-York-Milano: McGraw Hill, 2016

[127] De Vita, Hellmann, Lawrence. Rosenberg's Cancer: Principles & Practice of Oncology.Lippincott Williams & Wilkins, 2008.

[128] Park Y, Spiegelman D, Bergkvist L, Berrino F, van den Vrandt PA, Buring JE, Colditz GA, Freudnheim JL., Kato I, Krogh V, Leitzmann MF, McCullough ML, Miller AB, Pietinen P, Rohan TE, Schatzkin A, Willett WC, Wolk A, Zeleniuch-Jacquotte A, Zhang SM, Smith Warner SA. Dietary fiber intake and risk of colorecgtal cancer: a pooled analysis of prospective cohort studies. JAMA 2005, 294:2849-2857

[129] Gregory L, Brotzman.Colorecgtal cancer Risk Factors. Colorectal Cancer 2006.

[131] Kim JB. Three-dimensional tissue culture models in cancer biology. Semin Cancer Biol 2005; 15:365-377

[130] Aranzazu Villasante, and Gordana Vunjak-Novakovic, "Tissue-engineered models of human tumors for cancer research," *Expert Opin Drug Discov.*, vol. 10, no. 3, pp. 257–268, 2015.

[131] D. R. Pattabiraman and R. A. Weinberg, "Tackling the cancer stem cells - what challenges do they pose?," *Nat Rev Drug Discov*, vol. 13, no. 7, pp. 497–512, 2014.

[132] A. G. Clark and D. M. Vignjevic, “Modes of cancer cell invasion and the role of the microenvironment,” *Curr. Opin. Cell Biol.*, vol. 36, pp. 13–22, 2015.

[133] P. Friedl and S. Alexander, “Cancer invasion and the microenvironment: Plasticity and reciprocity,” *Cell*, vol. 147, no. 5, pp. 992–1009, 2011.

[134] G. Imparato, F. Urciuolo, and P. A. Netti, “*In vitro* three-dimensional models in cancer research: a review,” *Int. Mater. Rev.*, vol. 60, no. 6, pp. 297–311, 2015.

[135] A. Nyga, U. Cheema, and M. Loizidou, “3D tumour models: Novel *in vitro* approaches to cancer studies,” *J. Cell Commun. Signal.*, vol. 5, no. 3, pp. 138 239–248, 2011

[136] E. C. Ilya Serebriiskii, Remedios Castelló-Cros, Acacia Lamb, Erica A. Golemis, “Fibroblast-derived 3D matrix differentially regulates the growth and drug-responsiveness of human cancer cells,” *Matrix Biol.*, vol. 27, no. 6, pp. 573–585, 2008.

[137] M. D. Amatangelo, D. E. Bassi, A. J. P. Klein-Szanto, and E. Cukierman, “Stroma-derived three-dimensional matrices are necessary and sufficient to promote desmoplastic differentiation of normal fibroblasts.,” *Am. J. Pathol.*, vol. 167, no. 2, pp. 475–488, 2005.

[138] Yamada KM, Cukierman E. Modeling tissue morphogeneis and cancer in 3D. Cell 2007; 130:601-610.

[139] Yuhas JM, Li AP, Martinez AO, Ladman AJ. A simplified method for production and growth of multicellular tumor spheroids. Cancer Res 1977; 37:3639-3643

[140] Sutherland RM. Cell environment interactions in tumora microregions: the multicell spheroid model. Science 1988; 240:177-184

[141] Brancato et al, Acta biomaterialia 47(2017) 1-13. 3D in not enough: Building up a cell ins tructive microenvironment for tumoral stroma microtissue.

[142] S. Yang, K. F. Leong, Z. Du, and C. K. Chua, "The design of scaffolds for use in tissue engineering. Part I. Traditional factors," *Tissue Eng.*, vol. 7, no. 6, pp. 679–689, Dec. 2001.

[143] Zachos NC, Kovbasnjuk O, Foulke-abel J, In J, Blutt SE, De Jonge HR, Estes MK: Human enteroids/colonoids and intestinal organoids functionally recapitulate and pathophysiology. J. Biol. Chem. 2016, 291:3759-3766.)

[144] C. Palmiero et al. / Acta Biomaterialia 6 (2010) 2548–2553

F. Rosso, G. Marino, A. Giordano, M. Barbarisi, D. Parmeggiani, and A. Barbarisi, "Smart materials as scaffolds for tissue engineering," *J. Cell. Physiol.*, vol. 203, no. 3, pp. 465–470, Jun. 2005.

[145] K. J. Livak and T. D. Schmittgen, "Analysis of relative gene expression data using real-time quantitative PCR and the 2(-Delta Delta C(T)) Method.," *Methods*, vol. 25, no. 4, pp. 402–8, Dec. 2001.

[146] Saville M, Lietzau J, et al. Treatment of HIV-associated Kaposi's sarcoma with paclitaxel. Lancet 1995 26-28

[147] Ahmed AA, Wang X, Lu Z et al. Modulating microtubule stability enhances the cytotoxic response of cancer cells to paclitaxel.

[148] Mielgo A, Torres VA, Clair K, Barbero S, Stupack DG. Paclitaxel promotes a caspase 8-mediated apoptosis through death

effector domain association with microtubules. *Oncogene*. 2009;28(40):3551–3562.

[149] Moktan S, Ryppa C, Kratz F, Raucher D. A thermally responsive biopolymer conjugated to an acid-sensitive derivative of paclitaxel stabilizes microtubules, arrests cell cycle, and induces apoptosis. *Invest New Drugs*. 2012;30(1):236–248.

[150] Peltier S, Oger J-M, Lagarce F, Couet W, Benoît J-P. Enhanced oral paclitaxel bioavailability after administration of paclitaxel-loaded lipid nanocapsules. *Pharm Res*. 2006;23(6):1243–1250.

[151] Bu H, He X, Zhang Z, Yin Q, Yu H, Li Y. A TPGS-incorporating
nanoemulsion of paclitaxel circumvents drug resistance in breast cancer.
Int J Pharm. 2014;471(1–2):206–213.

[152] Ganta S, Amiji M. Coadministration of paclitaxel and curcumin in to overcome multidrug resistance in tumor
cells. *Mol Pharm*. 2009;6(3):928–939.

[153] Choudhury H, Gorain B, Karmakar S, et al. Improvement of cellular uptake, in vitro antitumor activity and sustained release profile with increased bioavailability from a nanoemulsion platform. *Int J Pharm*. 2014;460(1–2):131–143.

[154] Dias ML, Carvalho JP, Rodrigues DG, Graziani SR, Maranhao RC. Pharmacokinetics and tumor uptake of a derivatized form of paclitaxel associated to a cholesterol-rich nanoemulsion (LDE) in patients with gynecologic cancers. *Cancer Chemother Pharmacol*. 2007;59(1): 105–111.

[155] Desai A, Vyas T, Amiji M. Cytotoxicity and apoptosis enhancement in brain tumor cells upon coadministration of paclitaxel

and ceramide in nanoemulsion formulations. *J Pharm Sci*. 2008;97(7):2745–2756.

[156] Lv et al, frontiers in pharmacology 2017.

[157] L Jin, GN Alesi, and S Kang, Glutaminolysis as a target for cancer therapy. *Oncogene* (2016) **35,** 3619–3625; doi:10.1038/onc.2015.447; 23 November 2015

[158] Hu J, Locasale JW, Bielas JH, O'Sullivan J, Sheahan K, Cantley LC, Vander Heiden MG, Vitkup D. Heterogeneity of tumor-induced gene expression changes in the human metabolic network. Nat Biotechnol. 2013 Jun;31(6):522-9. doi: 10.1038/nbt.2530. Epub 2013 Apr 21. PubMed PMID: 23604282; PubMed Central PMCID: PMC3681899.